HYDROLOGICAL PROCESSES
Hydrol. Process. **19**, 4121–4146 (2005)
Published online 1 August 2005 in Wiley InterScience (www.interscience.wiley.com). DOI: 10.1002/hyp.5876

Spatial distribution and seasonal variation in $^{18}O/^{16}O$ of modern precipitation and river water across the conterminous USA

Andrea Dutton,[1]* Bruce H. Wilkinson,[1] Jeffrey M. Welker,[2] Gabriel J. Bowen[3] and Kyger C. Lohmann[1]

[1] *Department of Geological Sciences, University of Michigan, Ann Arbor, MI 48109, USA*
[2] *Natural Resource Ecology Laboratory (NREL), Colorado State, Fort Collins, CO 80523, USA*
[3] *Department of Earth Sciences, University of Santa Cruz, Santa Cruz, CA 95064, USA*

Abstract:

We report a quantitative analysis of regional differences in the the oxygen isotope composition of river water and precipitation across the USA because data are now available to undertake a more geographically and temporally extensive analysis than was formerly possible. Maps of modern, mean annual $\delta^{18}O$ values for both precipitation ($\delta^{18}O_{PPT}$) and river water ($\delta^{18}O_{RIV}$) across the 48 contiguous states of the USA have been generated using latitude and elevation as the primary predictors of stable isotope composition while also incorporating regional and local deviations based on available isotopic data. The difference between these two maps was calculated to determine regions where $\delta^{18}O_{RIV}$ is significantly offset from local $\delta^{18}O_{PPT}$. Additional maps depicting seasonal and extreme values for $\delta^{18}O_{RIV}$ and $\delta^{18}O_{PPT}$ were also constructed.

This exercise confirms the presence of regions characterized by differences in $\delta^{18}O_{RIV}$ and $\delta^{18}O_{PPT}$ and specifically identifies the magnitude and regional extent of these offsets. In particular, the Great Plains has $\delta^{18}O_{RIV}$ values that are more positive than precipitation, while much of the western USA is characterized by significantly lower $\delta^{18}O_{RIV}$ values in comparison with local $\delta^{18}O_{PPT}$. The most salient feature that emerged from this comparison is the 'catchment effect' for the rivers. Because river water is largely derived from precipitation that fell upstream of the sample locality (i.e. at higher elevations) $\delta^{18}O_{RIV}$ values are often lower than local $\delta^{18}O_{PPT}$ values, particularly in catchments with high-elevation gradients. Seasonal patterns in the isotopic data substantiate the generally accepted notion that amplitudes of $\delta^{18}O$ variation are greatly dampened in river water relative to those of local precipitation. Copyright © 2005 John Wiley & Sons, Ltd.

KEY WORDS stable isotopes; oxygen; rivers; precipitation; meteoric water

INTRODUCTION

Oxygen isotope data for modern meteoric precipitation collected at mid- to high-latitude continental localities display a robust correlation with surface temperature (Dansgaard, 1964; Yurtsever and Gat, 1981; Rozanski *et al*., 1993). This relation is understood as recording the continual depletion of ^{18}O from water vapour as air masses move along temperature gradients toward higher latitudes, inland from coasts, or to higher elevations. Though geographic and climatic parameters (e.g. latitude, elevation, distance from coast, humidity) that control surface air temperature are largely correlative with $\delta^{18}O_{PPT}$ values (Dansgaard, 1964; Yurtsever and Gat, 1981; Rozanski *et al*., 1993), further investigations of factors controlling the oxygen isotope composition of precipitation indicate a complex interplay of processes (e.g. Lawrence and White, 1991a). For example, significant recycling of evaporated water (Salati *et al*., 1979; Gat and Matsui, 1991; Ingraham

* Correspondence to: Andrea Dutton, Research School of Earth Sciences, The Australian National University, 1 Mills Road, Canberra, ACT 0200, Australia. E-mail: andrea.dutton@anu.edu.au

Received 24 February 2004
Accepted 11 November 2004

and Taylor, 1991) or storm track trajectories that change over seasonal or longer time scales (Nativ and Riggio, 1990; Simpkins, 1995; Amundson *et al.*, 1996) can exert significant control over resultant $\delta^{18}O_{PPT}$ values.

These complications notwithstanding, numerous proxies for meteoric $\delta^{18}O$ in continental environments have been developed over the last several decades with the aim of making interpretations related to climate, ecology, and linkages between precipitation, surface, and groundwater flow in both modern and ancient environments. These include $\delta^{18}O$ measurements of ice cores (Dansgaard *et al.*, 1993; Thompson *et al.*, 1995; Petit *et al.*, 1999), speleothems (Schwarz, 1986; Dorale *et al.*, 1992; Denniston *et al.*, 1999), pedogenic carbonates (Cerling and Quade, 1993; Amundson *et al.*, 1996), groundwater (Rozanski, 1985; Dutton, 1995), meteoric calcite cements (Hays and Grossman, 1991), haematite coatings on bones (Bao *et al.*, 1998; Bao and Koch, 1999), authigenic clays (Chamberlain and Poage, 2000), and biogenic hard parts, such as freshwater molluscs (Dettman and Lohmann, 2000), fossil tooth enamel (Bryant *et al.*, 1996; Fricke *et al.*, 1998; Sharp and Cerling, 1998), and otoliths (Wurster and Patterson, 2001). Beyond ambiguities associated with the $\delta^{18}O_{PPT}$–temperature relation (Fricke and O'Neil, 1999), proxies for compositions of ancient meteoric precipitation are also complicated by indefinite relations between the composition of local precipitation and that of surface water (e.g. lakes, rivers) and/or groundwater. Without understanding the causes behind differences in the regional isotopic composition of modern precipitation and surface or groundwater today, it is difficult to explain the causes of climate change in the past from proxy data.

Local and sub-regional isotope hydrology studies have shown that the stable isotope ($\delta^{18}O$ or δD) composition of rivers can be substantially different than that of incident precipitation. These differences have been variously attributed to regional water budgets dominated by winter snowmelt at high elevations that is highly depleted in ^{18}O (Friedman *et al.*, 1992), regional effects of evapotranspiration that enrich surface waters in ^{18}O and deuterium (Simpson and Herczeg, 1991; Gremillion and Wanielista, 2000), and to water budgets that are dominated by winter isotopic compositions due to insufficient infiltration of precipitation during the warmer months when evapotranspiration is high and/or enhanced infiltration of winter precipitation under snowpack (Fritz *et al.*, 1987; Simpkins, 1995).

In this study we have compared the oxygen isotope compositions of precipitation and river water across the USA, drawing upon the large datasets that are now available. Though there may be similarities between river water and groundwater compositions, we leave the comparison of $\delta^{18}O_{PPT}$ and groundwater $\delta^{18}O$ for future work and focus upon the relationship between precipitation and river water compositions. The primary objectives of this study are: (1) to develop a spatially continuous model for mean annual $\delta^{18}O$ compositions of both meteoric precipitation and river water across the USA; (2) to compare $\delta^{18}O_{PPT}$ and $\delta^{18}O_{RIV}$ values quantitatively; (3) to generate maps displaying annual seasonal variation in $\delta^{18}O_{PPT}$ and $\delta^{18}O_{RIV}$; (4) to evaluate driving mechanisms responsible for regional patterns of difference and similarity between $\delta^{18}O_{PPT}$ and $\delta^{18}O_{RIV}$; (5) to assess the legitimacy of using proxies of surface water $\delta^{18}O$ values in order to make palaeoclimatic and hydrologic interpretations in modern and ancient environments. To achieve these goals we have drawn upon the Coplen and Kendall (2000) dataset of river compositions, data from the Global Network for Isotopes in Precipitation (GNIP; IAEA/WMO, 2001), United States Network of Isotopes in Precipitation (USNIP; Welker, 2000; Welker *et al.*, 2002), as well as additional published data (Krabbenhoft, 1990; Nativ and Riggio, 1990; Kendall, 1993; Simpkins, 1995; Winograd *et al.*, 1998; Frederickson and Criss, 1999; Coplen and Huang, 2000; Harvey and Welker, 2000) to generate maps of precipitation and river water $\delta^{18}O$ across the USA. Instead of contouring the data, a model was developed that predicts $\delta^{18}O$ values primarily on the basis of geographic parameters (latitude and elevation), but also incorporates other regional factors that influence water isotope composition. This procedure allows for the generation of continuous grid maps with a spacing of 30 arc-seconds that display estimates of modern precipitation and river $\delta^{18}O$.

MODEL DERIVATION AND RESULTS

Oxygen isotope data

Oxygen isotope data for all waters discussed herein are reported in permil relative to Vienna Standard Mean Ocean Water (VSMOW; Gonfiatini, 1978). River water $\delta^{18}O$ data were generated by Coplen and Kendall (2000) from samples collected through the United States Geological Survey (USGS) National Stream Quality Accounting Network (NASQAN) and Hydrologic Benchmark Network (HBN) programmes. These data were collected at bimonthly to quarterly intervals. Stations with too few measurements to resolve seasonal variation in river isotope composition were excluded from this analysis. Kendall and Coplen (2001) provide a detailed description and analysis of this dataset.

$\delta^{18}O_{PPT}$ data are provided by both the GNIP database (accessible at: http://isohis.iaea.org) and the USNIP dataset (IAEA/WMO, 2001; Welker *et al*., 2002). The GNIP database includes compositions from 583 stations, although fewer than half have records spanning more than 1 year (Rozanski *et al*., 1993). The USNIP database was generated using archived precipitation samples from the National Atmospheric Deposition Program (NADP; Harvey and Welker, 2000; Welker *et al*., 2002). These two datasets were augmented by a compilation of precipitation data with seasonal resolution (Krabbenhoft, 1990; Nativ and Riggio, 1990; Kendall, 1993; Simpkins, 1995; Winograd *et al*., 1998; Frederickson and Criss, 1999; Coplen and Huang, 2000; Harvey and Welker, 2000). Precipitation data drawn from the literature were collected on weekly, monthly, or quarterly time intervals (depending upon the author), and span at least 1 year, such that at least one full annual cycle of variation is recorded at each locality.

Mean annual $\delta^{18}O_{PPT}$ and $\delta^{18}O_{RIV}$ values were calculated as averages that are unweighted with respect to the amount of precipitation or river discharge due to insufficient precipitation amount data in the aforementioned data sources during the periods of sample collection. Because seasonal imbalances in precipitation amount can significantly impact the resultant isotopic composition of surface water reservoirs, long-term averages of seasonal precipitation amounts are used to qualitatively interpret differences in the maps of unweighted $\delta^{18}O_{PPT}$ and $\delta^{18}O_{RIV}$. Finally, to facilitate comparison of $\delta^{18}O_{PPT}$ and $\delta^{18}O_{RIV}$ across geographic space and through annual cycles of variation we must extrapolate the existing datasets through both space and time.

Temporal interpolation

In many studies, mean annual and seasonal variation in $\delta^{18}O$ is determined as the arithmetic mean and range of all, often monthly, data. This approach, however, presumes that all months are equally represented by $\delta^{18}O$ data; if not, data from those years represented by less than 12 months of data are commonly discarded. Such an approach may result in a significant loss of information. In addition, when amplitudes of seasonal variation are based on the extremes in monthly compositions over a 12 month interval, the fidelity of such estimates is entirely conditional on frequency of sampling and the amount of noise in the data, and will suffer from statistical uncertainty associated with using only a few data points to calculate a year-long quantity. Using the mean difference between all seasonal highs and lows alleviates this problem to some degree, but does not obviate uncertainty associated with identifying seasonal peaks and troughs.

In light of these problems associated with estimation of means and seasonal ranges in isotope composition, we determined these two metrics by iteratively computing the best-fit sinusoid through successive subsets of monthly $\delta^{18}O_{PPT}$ and $\delta^{18}O_{RIV}$ data. The sine curve regression method employed herein and the validity of applying this method to seasonal $\delta^{18}O$ data at mid- to high-latitudes is discussed in detail by Wilkinson and Ivany (2002). Using this technique, mean position of the best-fit sine curve for each sampling locality represents mean annual isotopic composition, and sine amplitude reflects the seasonal range of compositional variation. Means and amplitudes can be derived in this fashion from time intervals represented by somewhat incomplete data, and magnitudes of seasonal variation are less dependent on short-term deviations from the annual signal. Moreover, all data points contribute equally to constrain the mean position and shape of the sine curve.

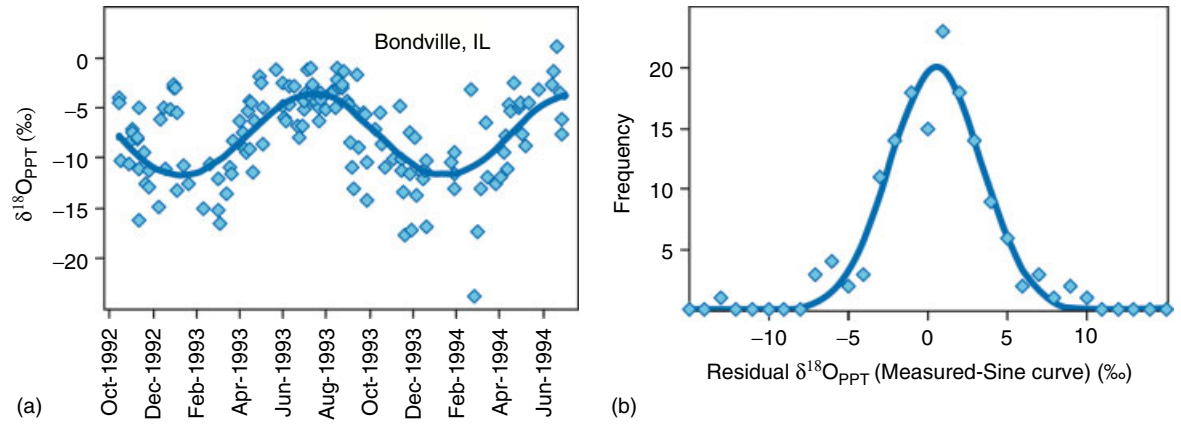

Figure 1. Isotope compositions of 150 precipitation samples from the Bondville, IL (a) and frequency of differences between compositions and a best-fit sinusoid (b). (a) Temporal variation in water sample compositions collected at approximately 4-day intervals from 14 October 1992 until 26 June 1996. This interval spans approximately 1·7 years of seasonal temperature and water composition change. Sinusoid mean composition is −7·7‰; seasonal amplitude is 7·8‰. (b) Frequency distribution of differences between measured sample and annual sine variation in water compositions. Note that the distribution of residuals is essentially Gaussian (line). The residual mean is 0·6‰ with a standard deviation of 2·9‰. This figure is available in colour online at http://www.interscience.wiley.com/hyp

Best-fit sine curves were determined for successive subsets or windows of data, advancing the window by 1 month, and repeating the procedure until the entire dataset has been processed. Window sizes spanned approximately one wavelength (12 months) of variation. Best-fit sinusoids of annual $\delta^{18}O$ variation were determined for every station represented by at least 13 months of data, and were done so for all possible time intervals that also contained data gaps of no more than six consecutive months. Residuals between measured $\delta^{18}O$ and the sine-curve fit are essentially Gaussian noise, and suggest that determination of best-fit sinusoids accurately captures *average* maximum and minimum $\delta^{18}O$ values during an annual cycle. This behaviour is illustrated with a sinusoid fit for $\delta^{18}O_{PPT}$ data from Bondville, IL (Coplen and Huang, 2000) (Figure 1a). Note that the frequency distribution of differences between measurements and the sinusoid fit is Gaussian (Figure 1b). Similar sine curves were generated for each station corresponding to precipitation and river water data used in this study.

For comparison, we also computed arithmetic means of monthly $\delta^{18}O$ data, as well as estimates of seasonal change in $\delta^{18}O$ using the difference between extreme minimum and maximum values reported for each station. Owing to the fact that monthly data from most stations are evenly distributed throughout the year, little difference exists between sinusoidal and arithmetic means (Figure 2). However, many stations display rather substantial differences between magnitudes of seasonal variation estimated from sine amplitudes versus the range between minimum and maximum values reported (Figure 3). These differences exist because sine amplitude is relatively insensitive to the standard deviation of Gaussian noise about the annual signal, whereas the absolute range of reported values depends greatly on both the sampling frequency and on the noise inherent in local climatic conditions. Because both representations of seasonality are useful for palaeoclimatologists, we report seasonal variation in $\delta^{18}O$ both in terms of the sine amplitudes and the total range of measured values.

Spatial interpolation

Previous studies have established that spatial variation in the isotope composition of meteoric water is primarily dependent upon latitude, elevation, distance from the coast, rain-out (amount effect), the seasonal balance derived from different sources, and recycling of evaporated water (Dansgaard, 1964; Sheppard *et al.*, 1969; Nativ and Riggio, 1990; Rozanski *et al.*, 1993). Comparison of compositions of meteoric precipitation and river water at any location has traditionally been accomplished by linear interpolation between sampling

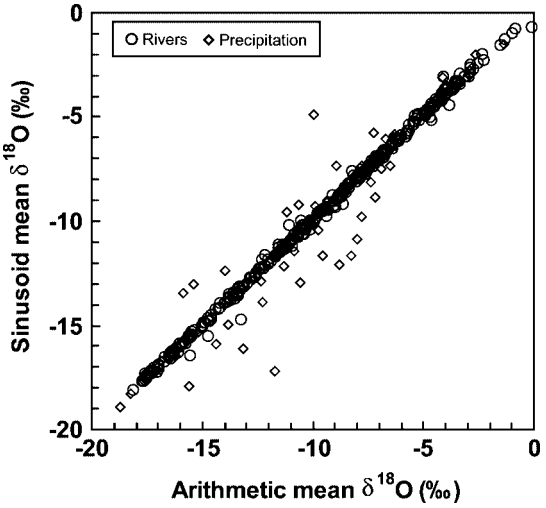

Figure 2. Sinusoid mean versus arithmetic mean for precipitation (diamonds) and river water (circles) $\delta^{18}O$ data plot on a 1:1 line. The precipitation data show more scatter because there is greater seasonality and, therefore, variability in the $\delta^{18}O$ data than for river water

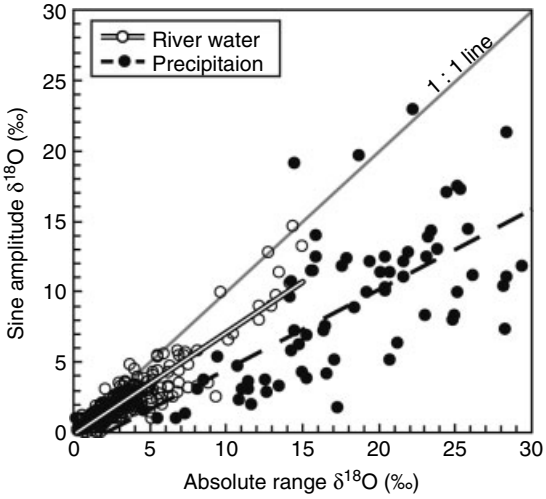

Figure 3. Sine amplitude versus total range of $\delta^{18}O$ for precipitation (solid circles) and river water (open circles). The sine amplitudes are consistently smaller than the total range because the sinusoid computes average minimum and maximum annual values, whereas the total range reflects the extreme compositions recorded. River water samples fall closer to the 1 : 1 line than precipitation samples because there is less noise in the annual variability of $\delta^{18}O$

stations, or by reference to the nearest station. If we analyse our compiled datasets using this method of reference to the nearest station, 20 pairs of sampling stations can be identified where the distance separating the precipitation and riverine stations is <50 km (Table I). Differences in $\delta^{18}O$ mean and total range are quite large in some cases, and negligible in others. Unfortunately, the frequency of significant differences in these parameters is difficult to evaluate for the entire USA based on such a limited number of samples. Moreover, conclusions made solely from this analysis would be highly dependent upon the location (spatial distribution) of these stations, the comparison does not account for local heterogeneities in elevation and/or climate that might exist between sampling localities, and is limited to only a few examples due to the spacing of available

Table I. Comparison of $\delta^{18}O_{PPT}$ and $\delta^{18}O_{PPT}$ values for pairs of stations within a 50 km radius

Pair #	Distance (km)	River station	Precipitation station	Location name	LAT (°)	LON (°)	Elev. (m)	Mean (‰)	Range (‰)	ΔMean (‰)	ΔRange (‰)
1	19·0	12 040 500[f]		Queets River near Clearwater, WA	47·54	−124·31	4	−9·7	1·0	−2·7	−7·6
			7 420 500[a]	Destruction Island, WA	47·70	−124·50	21	−7·0	8·6		
2	16·9	14 306 500[f]		Alsea River near Tidewater, OR	44·39	−123·83	15	−8·3	0·7	−0·9	−11·8
			OR-02[b]	Alsea, OR	44·39	−123·62	104	−7·4	12·5		
3	43·0	12 101 500[f]		Puyallup River at Puyallup, WA	47·21	−122·34	32	−12·4	2·9	−2·8	−7·9
			WA-21[c]	La Grande, WA	46·84	−122·29	617	−9·6	10·8		
4	26·5	11 447 650[f]		Sacramento River at Freeport, CA	38·45	−121·50	1	−10·9	0·6	−3·8	−10·5
			CA-88[c]	Davis, CA	38·5	−121·80	18	−7·1	11·1		
5	27·0	11 264 500[f]		Merced River near Yosemite, CA	37·73	−119·56	1224	−13·0	2·8	−3·1	−13·8
			CA-99[c]	Yosemite NP, CA	37·9	−119·90	2298	−9·9	16·5		
6	44·7	13 342 500[f]		Clearwater River at Spalding, ID	46·45	−116·83	235	−15·5	1·5	−3·0	−10·0
			WA-24[c]	Palouse Conservation Fm, WA	46·76	−117·18	766	−12·4	11·5		
7	45·7	10 244 950[f]		Steptoe Creek near Ely, NV	39·20	−114·69	2268	−15·9	0·3	−4·6	−28·1
			NV-05[c]	Great Basin NP, NV	39·01	−114·22	2067	−11·3	28·4		
8	21·5	12 363 000[f]		Flathead River at Columbia Falls, MT	48·36	−114·18	908	−16·9	0·3	−3·8	−15·3
			MT-05[c]	Glacier NP, MT	48·51	−114·00	968	−13·1	15·6		
9	2·4	9 315 000[f]		Green River at Green River, UT	38·99	−110·15	1231	−15·6	3·7	−6·8	−24·7
			UT-98[c]	Green River, UT	39·00	−110·20	1244	−8·8	28·4		
10	27·3	9 251 000[f]		Yampa River near Maybell, CO	40·50	−108·03	1798	−16·4	2·9	−4·1	−15·0
			CO15[c]	Sand Spring Creek, CO	40·51	−107·70	1998	−12·3	17·9		
11	47·2	8 481 500[f]		Rio Tularosa near Bent, NM	33·14	−105·90	1661	−8·8	0·3	−1·6	−21·3
			NM-08[c]	Mayhill, NM	32·90	−105·50	2009	−7·2	21·6		
12	33·3	6 409 000[f]		Castle Creek, SD	44·01	−103·83	1801	−16·1	0·55	−2·3	−23·0
			WY-99[c]	Newcastle, WY	43·87	−104·19	1466	−13·8	23·5		

13	2·3	6 337 000[f]		Little Missouri River, ND	47·59	−103·25	588	−13·2	12·8	−1·5	−9·4
			ND-07[c]	Theodore Roosevelt NP, ND	47·60	−103·26	611	−11·7	22·2		
14	46·4	8 210 000[f]		Nueces River near Three Rivers, TX	28·44	−98·19	31	−2·8	3·6	1·5	−1·0
			TX-03[c]	Beeville, TX	28·50	−97·71	82	−4·4	4·6		
15	48·3	5 102 500[f]		Red River at Emerson, Manitoba	49·01	−97·21	213	−8·2	8·9	2·7	−7·7
			ND-08[c]	Icelandic State Park, ND	48·80	−97·75	306	−10·9	16·6		
16	5·4	6 879 650[f]		Kings Creek near Manhattan, KS	39·10	−96·60	346	−6·8	0·4	3·1	−14·1
			KS-31[c]	Konza Prairie, KS	39·10	−96·66	350	−10·0	14·5		
17	23·8	6 800 500[f]		Elkhorn River at Waterloo, NE	41·29	−96·28	337	−8·3	5·0	−0·9	N/A
			NE-15[d]	Mead, NE	41·20	−96·49	351	−7·4	N/A		
18	28·2	3 276 500[f]		Whitewater River at Brookville, IN	39·41	−85·01	182	−7·3	0·9	0·9	−22·2
			OH-09[e]	Oxford, OH	39·50	−84·72	284	−8·1	23·0		
19	47·7	2 327 100[f]		Sopchoppy River near Sopchoppy, FL	30·13	−84·49	0	−3·1	1·9	−0·26	−3·6
			FL-14[c]	Quincy, FL	30·50	−84·60	60	−2·8	5·5		
20	8·0	3 535 912[f]		Clinch River at Melton Hill Dam, TN	35·89	−84·30	0	−6·2	2·2	0·5	−19·0
			TN-00[e]	Walker Branch Watershed, TN	36·00	−84·29	341	−6·7	21·2		

[a] IAEA/WMO (2001).
[b] Welker (2000).
[c] Welker *et al.* (2002).
[d] Harvey and Welker (2001).
[e] Coplen and Huang (2000).
[f] Coplen and Kendall (2000).

data across the USA. In order to estimate changes in either $\delta^{18}O_{PPT}$ or $\delta^{18}O_{RIV}$, it is first necessary to take these factors into account.

Therefore, we adopt the modelling approach of Bowen and Wilkinson (2002) in order to determine spatial variation in the isotope composition of meteoric precipitation and river water across the conterminous USA. This is done by: (1) determining the dependence of $\delta^{18}O$ on latitude and elevation; (2) applying this empirical relation to GTOPO30 (30 arc-second global digital elevation model (DEM) with elevation data spaced at ~1 km) to generate a grid map of $\delta^{18}O$ based on these parameters; (3) mapping residuals between the latitude–elevation model and observed $\delta^{18}O$ values; (4) adding model $\delta^{18}O$ and residual maps to generate a map of $\delta^{18}O$ across the USA. Bowen and co-workers (Bowen and Wilkinson, 2002; Bowen and Revenaugh, 2003) showed that this approach captures the majority of $\delta^{18}O_{PPT}$ variability through the explicit representation of the effects of latitude and elevation on $\delta^{18}O_{PPT}$ and the implicit representation of spatially variable effects such as continental and source area effects. In order to compare isotope compositions of precipitation and rivers, this procedure was applied to both types of data and is described below in a step-by-step fashion for precipitation data.

Latitude dependence of meteoric precipitation

Our initial approximation of spatial variation in $\delta^{18}O_{PPT}$ was based on isotope compositions of global precipitation from the IAEA/GNIP database. Mean annual $\delta^{18}O_{PPT}$ was calculated for all stations using the sinusoid curve-fitting method. A second-order polynomial best describes the dependence of mean annual $\delta^{18}O_{PPT}$ on latitude for all stations at less than 200 m in elevation ($r^2 = 0{\cdot}77$; Figure 4a).

$$\delta^{18}O_{GNIP<200} = -0{\cdot}0055|LAT|^2 + 0{\cdot}2012|LAT| - 4{\cdot}7791 \quad (1)$$

where LAT is the latitude in decimal degrees, and $\delta^{18}O_{GNIP<200}$ is the oxygen isotope composition of precipitation from the IAEA/GNIP (global) database for all stations below 200 m in elevation. This elevation limit was chosen because there is no significant relation between $\delta^{18}O$ and elevation below 200 m. Negative

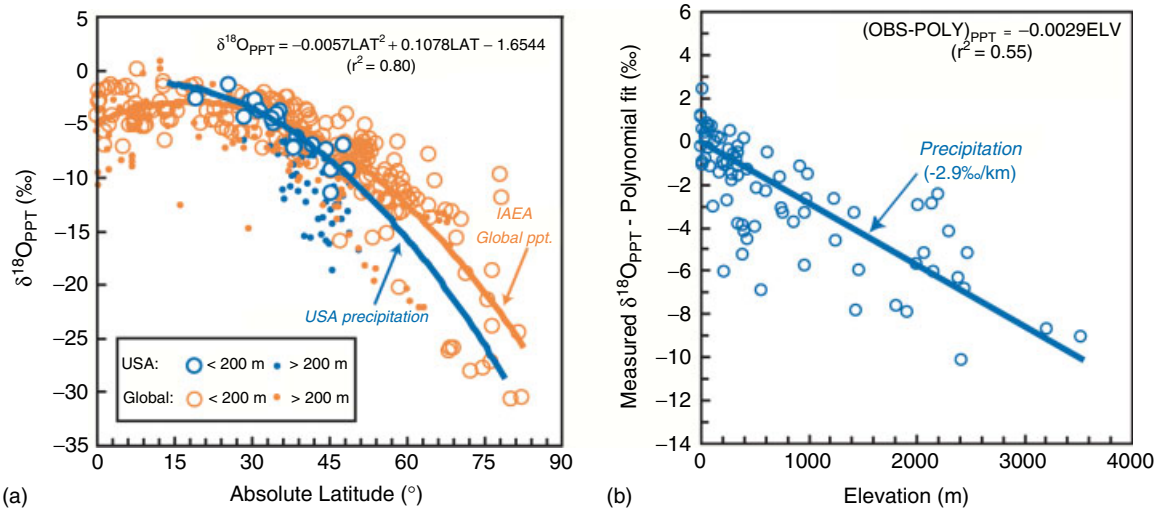

Figure 4. (a) $\delta^{18}O_{PPT}$ for the IAEA/GNIP database and for stations within or near the conterminous USA versus latitude. Rate of depletion in ^{18}O with increasing latitude is greater for stations in the USA in comparison with the global rate of depletion. The quadratic curve fit is applied to the low-elevation stations (<200 m), represented by open circles. High-elevation stations (≥200 m) are represented by solid circles. (b) The difference between measured $\delta^{18}O_{PPT}$ and $\delta^{18}O$ predicted by the second-order polynomial for US stations versus elevation. Slope of the regression (line) is the $\delta^{18}O_{PPT}$ lapse rate: −2·9‰ km^{-1}. This figure is available in colour online at http://www.interscience.wiley.com/hyp

correlation between precipitation $\delta^{18}O$ and station latitude results from the cooling and distillation of low-latitude water vapour during poleward transport.

To determine whether the trend of changing composition with latitude derived from the global database is a reasonable representation for individual continental air masses, these data were replotted by separating out $\delta^{18}O$ values for North America and Europe. This comparison demonstrates that European isotope compositions are more positive than those for North American data at comparable latitudes, and that the trend determined from the global dataset lies between trends defined from these two continents. Heavier compositions over Europe probably derive from different sources of water vapour; European precipitation is largely sourced from warm Gulf Stream waters, which impart a positive $\delta^{18}O$ signature to the precipitation.

Because of these differences, precipitation data from outside of North America were excluded in order to assess the influence of latitude and elevation on the composition of precipitation over the USA better. However, because this exclusion results in only 17 IAEA stations located within or near the contiguous USA, we also included $\delta^{18}O$ data compiled from the literature (17 stations), and from the USNIP (45 stations). Sinusoid mean annual $\delta^{18}O_{PPT}$ was calculated for each of these 79 sampling stations. Relative to latitude, the isotope composition of precipitation in the USA (including a few stations located outside of the USA, but near the Mexican or Canadian border) (Figure 4a) is described as

$$\delta^{18}O_{PPT<200} = -0{\cdot}0057LAT^2 + 0{\cdot}1078LAT - 1{\cdot}6544 \quad (2)$$

($r^2 = 0{\cdot}80$), where $\delta^{18}O_{PPT<200}$ is the oxygen isotope composition of precipitation in the USA for stations located below 200 m in elevation.

Elevation dependence of $\delta^{18}O_{PPT}$

In addition to latitude-related depletion, $\delta^{18}O_{PPT}$ values for the 58 stations above 200 m become increasingly depleted with increasing elevation, a change that primarily reflects the influence of Rayleigh distillation of water vapour as air masses orographically rise and cool. This effect of elevation on $\delta^{18}O_{PPT}$ is readily seen from the negative correlation between isotope composition and elevation, and as quantified by least-squares regression of station elevations and the residuals from Equation (2) ($r^2 = 0{\cdot}55$; Figure 4b):

$$RES_{PPT} = -0{\cdot}0029ELV \quad (3)$$

where RES_{PPT} (‰) is the difference between measured $\delta^{18}O_{PPT}$ and that predicted by Equation (2), ELV is elevation of the sampling station in metres, and the intercept is set to zero. The slope of this relation ($-2{\cdot}9$‰ km^{-1}) is the $\delta^{18}O_{PPT}$ lapse rate for North American precipitation. This is close to the average global oxygen isotope lapse rate of $-2{\cdot}8$‰ km^{-1} reported by Poage and Chamberlain (2001), but it is slightly larger in magnitude than the global average of $-2{\cdot}1$‰ km^{-1} calculated using this same method with the GNIP database (Bowen and Wilkinson, 2002).

In spite of this agreement, it should be noted that the North American $\delta^{18}O_{PPT}$ lapse rate was calculated from only 58 stations between 0·2 and 3·5 km in elevation; of these, 43 are located in the western USA (west of $-97°$ longitude). Moreover, $\delta^{18}O_{PPT}$ lapse rate may vary spatially and temporally due to differences: (1) between the eastern and western USA; (2) between individual mountain ranges; (3) between different sides of individual ranges, reflecting a rain-shadow effect (Coplen, 1993); and/or (4) between climate states such as El Niño or La Niña (Welker *et al.*, 2002). Because we apply a single oxygen isotope lapse rate ($-2{\cdot}9$‰ km^{-1}) to the entire country, our model somewhat oversimplifies such local complexity in the $\delta^{18}O_{PPT}$ signal.

The combined dependence of latitude and elevation on isotope compositions is described by adding Equations (2) and (3), and provides a reasonably good first-order estimate of observed $\delta^{18}O_{PPT}$ ($r^2 = 0{\cdot}79$; Figure 5a):

$$\delta^{18}O_{PPT} = -0{\cdot}0057LAT^2 + 0{\cdot}1078LAT - 1{\cdot}6544 - 0{\cdot}0029ELV \quad (4)$$

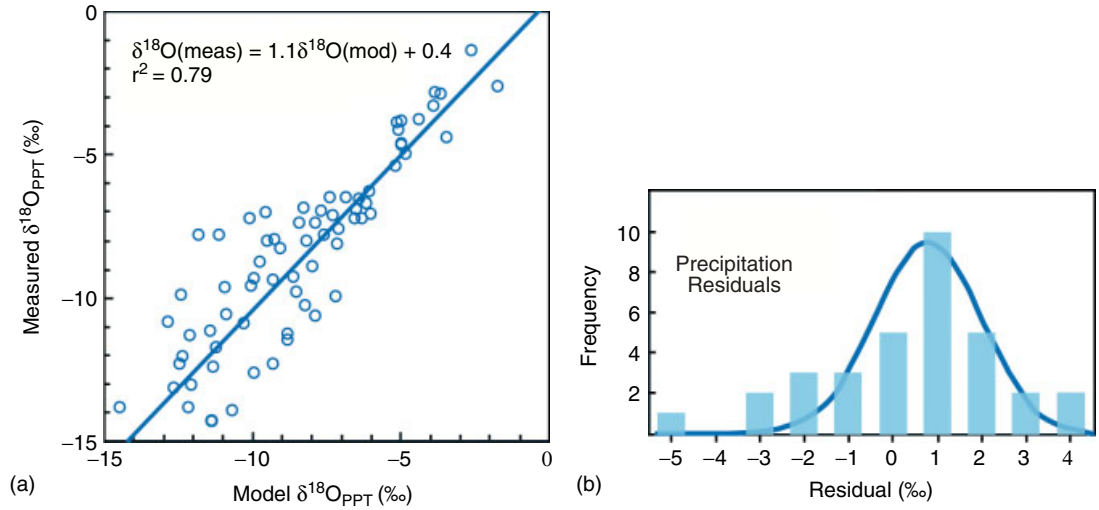

Figure 5. (a) Measured $\delta^{18}O_{PPT}$ versus $\delta^{18}O_{PPT}$ predicted by the latitude–elevation model (Equation (4)). (b) The frequency distribution of residuals between measured and model $\delta^{18}O_{PPT}$ for 79 stations. The line is the best-fit Gaussian distribution through these residuals, with a mean of −0·3‰ and standard deviation of 1·8‰. This figure is available in colour online at http://www.interscience.wiley.com/hyp

Differences between predicted and observed $\delta^{18}O_{PPT}$ values range from −5·4 to +4·0‰, with a standard deviation σ of 1·8‰ and a mean of −0·3‰ (Figure 5b). These residuals reflect the importance of other factors that influence meteoric $\delta^{18}O_{PPT}$, such as distance from vapour source ('continental effect'), precipitation rate ('amount effect'), storm-track trajectory, and relative humidity, that are not accounted for by only considering station latitude and elevation. In order to incorporate the combined influence of these regionally important processes, we contoured the residuals using an inverse-distance-weighted routine with a radius of 550 km (power: 2), the minimum distance required to produce a continuous contour surface across the USA. Kriging was not used to interpolate values because the data are not sufficiently continuous spatially to compute a semi-variogram model. A map of these residuals (Figure 6) displays differences between measured $\delta^{18}O_{PPT}$ and values predicted solely from station latitude and elevation.

To combine the influences of latitude and elevation upon $\delta^{18}O_{PPT}$ with the effects related to regional processes, $\delta^{18}O_{PPT}$ values anticipated from Equation (4) were then added to the residuals in Figure 6 to produce a map of $\delta^{18}O_{PPT}$ across the USA (Figure 7a). Latitude and elevation data for the contiguous USA were drawn from the GTOPO30 DEM, which provides satellite-generated elevation data spaced at 30 arc-seconds (∼1 km). This map of $\delta^{18}O_{PPT}$ differs from previously published maps of meteoric water composition (Dansgaard, 1964; Sheppard *et al.*, 1969; Yurtsever and Gat, 1981; Rozanski *et al.*, 1993; IAEA/WMO, 2001; Bowen and Wilkinson, 2002; Bowen and Revenaugh, 2003) primarily as a result of the greatly increased spatial density of data stations across the interior of the country.

Latitude and elevation dependence of river water $\delta^{18}O$

We have taken a nearly identical approach to generate a map of variation in river water $\delta^{18}O$ across the USA. Sinusoid mean annual $\delta^{18}O$ was calculated for 360 river stations included in the USGS NASQAN and HBN, as published by Coplen and Kendall (2000). Variation in $\delta^{18}O_{RIV}$ with latitude of 184 low-elevation (<200 m) stations is best described by the second-order polynomial

$$\delta^{18}O_{RIV<200} = -0{\cdot}0065LAT^2 - 0{\cdot}0016LAT + 3{\cdot}2103 \quad (5)$$

where $\delta^{18}O_{RIV<200}$ is the oxygen isotope composition of all river water stations collected below 200 m in elevation ($r^2 = 0{\cdot}72$; Figure 8a). As with $\delta^{18}O_{PPT}$, river stations at higher elevations frequently exhibit $\delta^{18}O_{RIV}$

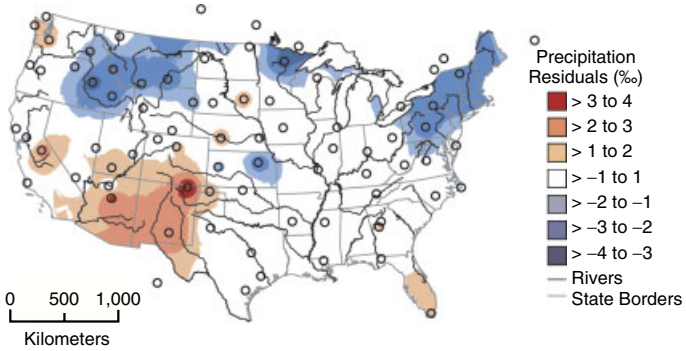

Figure 6. Residuals from the latitude–elevation model (see Figure 5b) contoured using an inverse-distance-weighted method. Note positive residuals (measured values are greater than predicted) centred over the arid southwest and southern Florida; negative residuals occur over portions of the northern USA

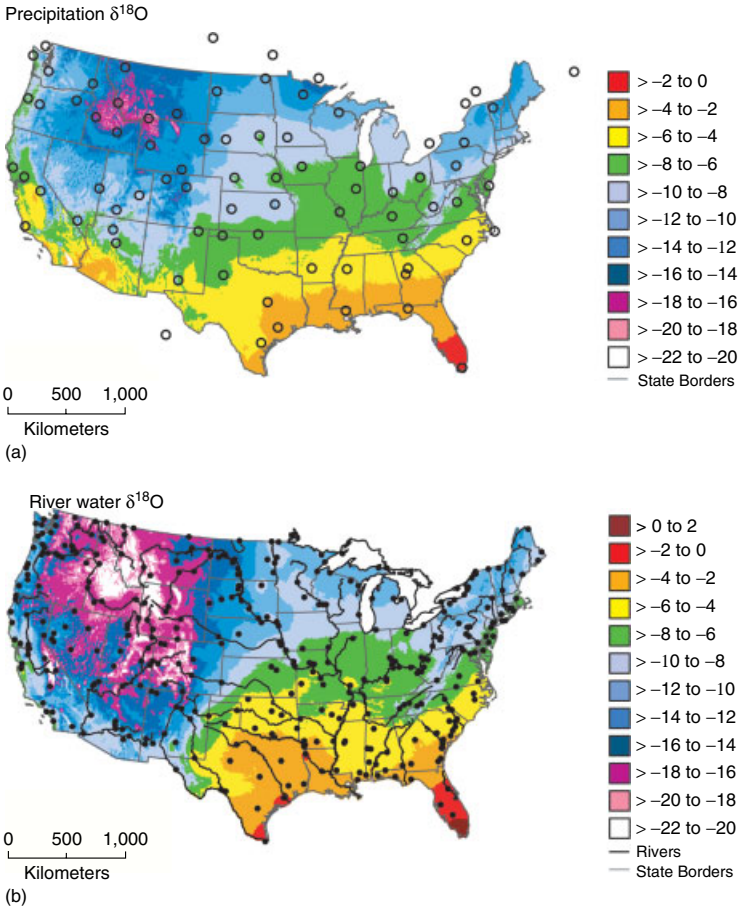

Figure 7. Unweighted, annual average isotope compositions of precipitation (a) and river water (b) across the contiguous USA. (a) Compositions of meteoric precipitation derived by adding the residual map (Figure 6) to $\delta^{18}O_{PPT}$ values calculated from latitude–elevation dependence of $\delta^{18}O_{PPT}$ (Equation (4)) and latitude–elevation data from GTOPO30 DEM. Sampling stations shown as open circles. (b) Compositions of river water from the addition of the residual map (Figure 10) to $\delta^{18}O_{RIV}$ values from the latitude–elevation (Equation (8)) and data from GTOPO30 DEM. River sampling stations denoted by solid circles. Major rivers of the USA are also shown for reference

values more negative than predicted by Equation (5); differences primarily reflect the effects of higher altitude (and lower temperature) on water compositions.

The magnitude of this effect can be quantified by plotting the residual $\delta^{18}O_{PPT}$ values versus collection station elevation ($r^2 = 0{\cdot}61$; Figure 8b), yielding the relation

$$RES_{RIV} = -0{\cdot}0042ELV \tag{6}$$

where RES_{RIV}(‰) is the difference between measured $\delta^{18}O_{RIV}$ and that predicted by Equation (5), ELV is elevation of the sampling station in metres, and the intercept is set to zero.

Interestingly, the elevation dependence of river water $\delta^{18}O$ predicted by Equation (6) is $-4{\cdot}2$‰ km^{-1}, a rate about 1·5 times the lapse rate we derived for precipitation ($-2{\cdot}9$‰ km^{-1}). Though we refer to Equation (6) as a 'lapse rate' for river water throughout the text, we emphasize that river water compositions are dependent upon many factors and that this apparent elevation dependence applies specifically to the river water stations of this dataset. As such, we caution against the application of this apparent 'lapse rate' to other scenarios.

Combining Equations (5) and (6) yields an expression for the net dependence of riverine isotope composition on latitude and elevation:

$$\delta^{18}O_{RIV} = -0{\cdot}0065LAT^2 - 0{\cdot}0016LAT + 3{\cdot}2103 - 0{\cdot}0042ELV \tag{7}$$

Comparison of measured $\delta^{18}O_{RIV}$ with values predicted by Equation (7) yields a good correlation ($r^2 = 0{\cdot}71$) between the two; these covary with a slope of 0·97, suggesting a near 1 : 1 relation between measured and model compositions (Figure 9). However, residuals between observed and model $\delta^{18}O_{RIV}$ have a somewhat larger range ($-7{\cdot}6$ to $+7{\cdot}4$‰) than $\delta^{18}O_{PPT}$ residuals (cf. Figures 9b and 5b), but exhibit similar standard deviations ($\sigma_{RIV} = 2{\cdot}0$‰; $\sigma_{PPT} = 1{\cdot}8$‰). As with $\delta^{18}O_{PPT}$ data, we then contoured residuals between observed $\delta^{18}O_{RIV}$ and values expected solely from station latitude and elevation (Equation (7)) for all 360 data localities using the same contouring parameters as for $\delta^{18}O_{PPT}$ data.

To evaluate spatial variation in $\delta^{18}O_{RIV}$ across the conterminous USA, data minus model residuals (Figure 10) were added to values anticipated from changes with latitude and elevation (Equation (7)) to

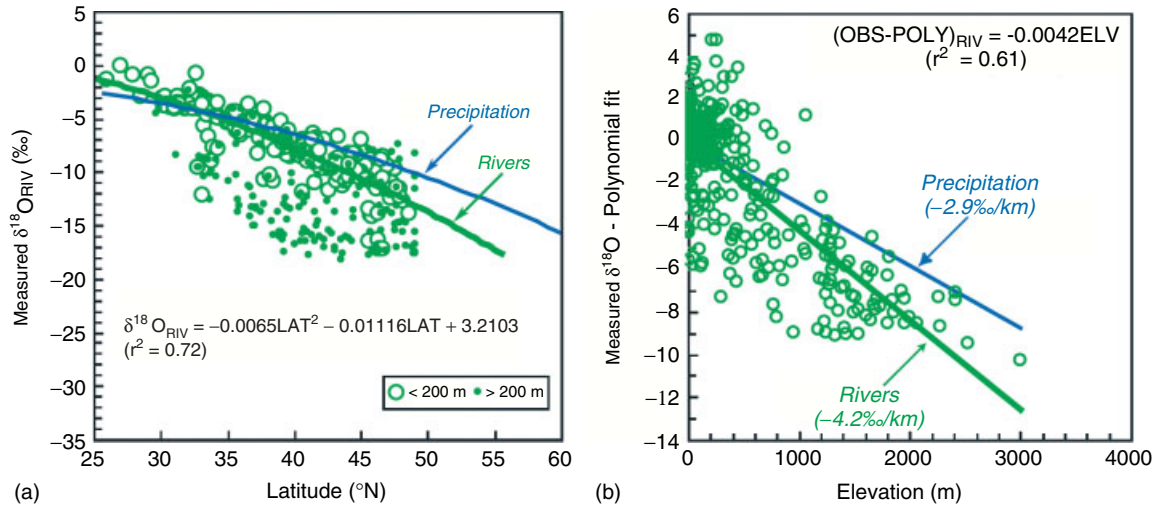

Figure 8. (a) $\delta^{18}O$ for rivers within the USA from Coplen and Kendall (2000). Quadratic curve (thick line) is for low-elevation stations (<200 m; open circles). Stations ≥200 m are shown as solid circles. The quadratic regression for precipitation (Equation (2); thin line) shown for comparison. (b) Differences between measured $\delta^{18}O_{RIV}$ and $\delta^{18}O_{RIV}$ predicted by the second-order polynomial (Equation (5)) versus river station elevation. Slope of the linear regression (thick line) is the oxygen isotope lapse rate for rivers ($-4{\cdot}2$‰ km^{-1}). Precipitation lapse rate ($-2{\cdot}9$‰ km^{-1}; thin line) shown for comparison. This figure is available in colour online at http://www.interscience.wiley.com/hyp

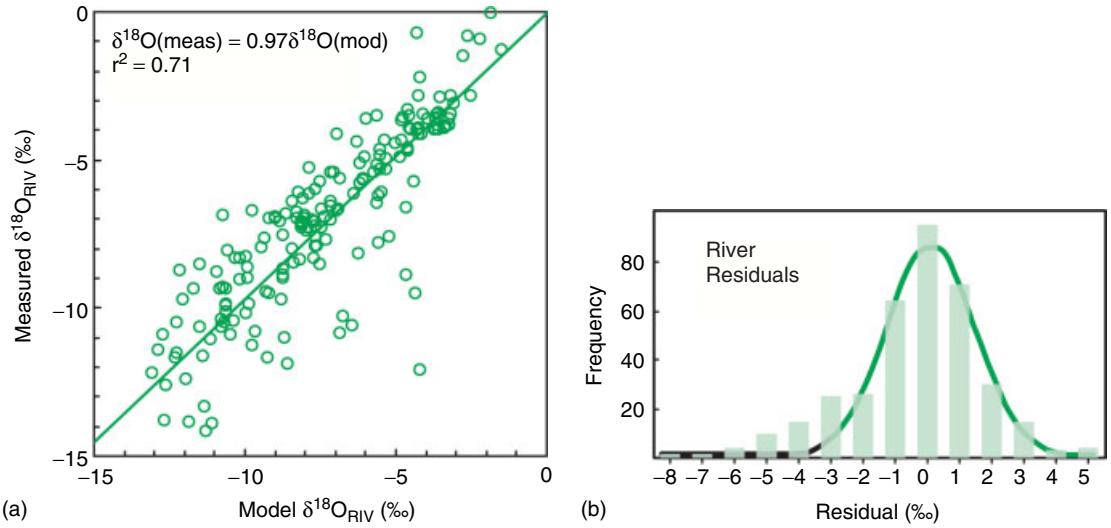

Figure 9. (a) Measured $\delta^{18}O_{RIV}$ versus values of $\delta^{18}O_{RIV}$ predicted by the latitude–elevation model (Equation (7)). (b) Frequency distribution of residuals between measured and model $\delta^{18}O_{RIV}$. The line is the best-fit Gaussian distribution through the residuals; the mean is 0·2‰ and the standard deviation is 2·0‰. This figure is available in colour online at http://www.interscience.wiley.com/hyp

generate a map of river water oxygen isotope compositions (Figure 7b). Riverine isotope compositions exhibit a gradual depletion of ^{18}O with increasing latitude and elevation, although ^{18}O depletion associated with increasing elevation is greater in magnitude for river water than for precipitation.

Spatial comparison of river water and precipitation $\delta^{18}O$

The final step in our analysis is to subtract the map of $\delta^{18}O_{PPT}$ (Figure 7a) from $\delta^{18}O_{RIV}$ (Figure 7b) to evaluate spatial similarities and/or differences between the stable isotope composition of precipitation and river water (Figure 11). Negative values that are largely centred over the western USA are areas where river water is more negative than local precipitation. Smaller regions of positive difference occur over the Great Plains and along coastal regions in southern Florida and New England. Much of the eastern USA is characterized by $\delta^{18}O_{PPT}$ and $\delta^{18}O_{RIV}$ values that are more or less equal (±1‰).

Comparison of seasonal variation in $\delta^{18}O$

As noted earlier, seasonal variation in $\delta^{18}O$ for each station was calculated in two ways: (1) as amplitudes of best-fit sinusoids through $\delta^{18}O_{PPT}$ data; (2) as absolute ranges of $\delta^{18}O_{PPT}$ and $\delta^{18}O_{RIV}$ data reported at each station. As might be expected, $\delta^{18}O_{PPT}$ sine amplitudes are consistently smaller than ranges in $\delta^{18}O_{PPT}$ values because sine minima and maxima represent averages of seasonal $\delta^{18}O$ extremes (Figure 3). Although sine amplitude for $\delta^{18}O_{PPT}$ and mean annual $\delta^{18}O_{PPT}$ covary, these parameters do not display covariation for river waters (Figure 12). A similar pattern results when plotting the arithmetic means and absolute ranges rather than the sinusoid amplitudes and means shown in Figure 12. The magnitude of $\delta^{18}O_{PPT}$ seasonality (sine amplitude and absolute range) generally increases with latitude, elevation, and distance from the coast (Figure 13). Seasonal variation in $\delta^{18}O_{RIV}$ is generally much smaller than the magnitudes observed for $\delta^{18}O_{PPT}$, and shows a higher magnitude of seasonality in the upper Midwest than in the rest of the country (Figure 14).

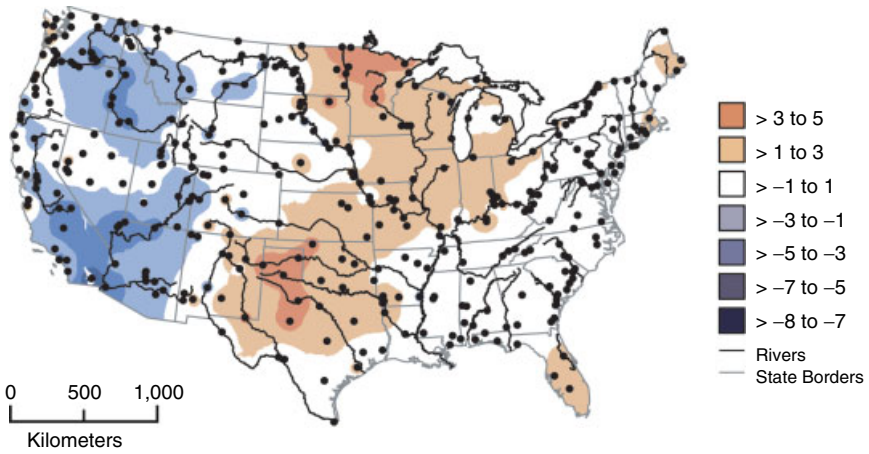

Figure 10. Residuals from the latitude–elevation model (Figure 9b) contoured using an inverse-distance-weighted method. Note positive residuals (measured values are higher than predicted) across the Great Plains, and negative residuals (measured values are lower than predicted) concentrated over the Columbia–Snake River basin, and the Colorado River basin

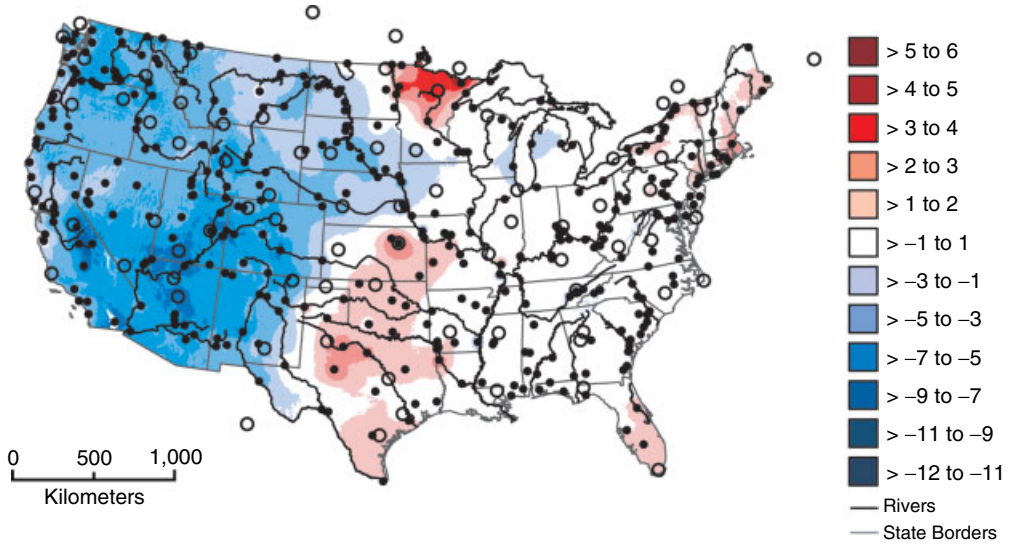

Figure 11. Differences between unweighted mean annual $\delta^{18}O_{PPT}$ (Figure 7a) and $\delta^{18}O_{RIV}$ (Figure 7b) calculated as ($\delta^{18}O_{RIV} - \delta^{18}O_{PPT}$). Positive anomalies (shades of red) denote regions where $\delta^{18}O_{RIV}$ is more positive than local $\delta^{18}O_{PPT}$; negative anomalies (shades of blue) are regions where $\delta^{18}O_{RIV}$ is more negative than local $\delta^{18}O_{PPT}$. Note that most of the eastern USA shows little difference (±1‰), but that substantial positive and negative anomalies occur across the Midwest and West. Precipitation stations are displayed as open circles; river water stations are shown with solid circles

DISCUSSION

Model assessment

Before evaluating the spatial patterns observed in the maps of meteoric $\delta^{18}O$, we first evaluate possible bias introduced by our modelling approach. The technique used here for spatial interpolation of meteoric $\delta^{18}O$ was first applied by Bowen and Wilkinson (2002) to generate a global $\delta^{18}O_{PPT}$ map, and has been statistically compared with other spatial interpolation techniques, including triangulation, inverse distance weighting, and Cressman objective analysis, by Bowen and Revenaugh (2003), who determined that the

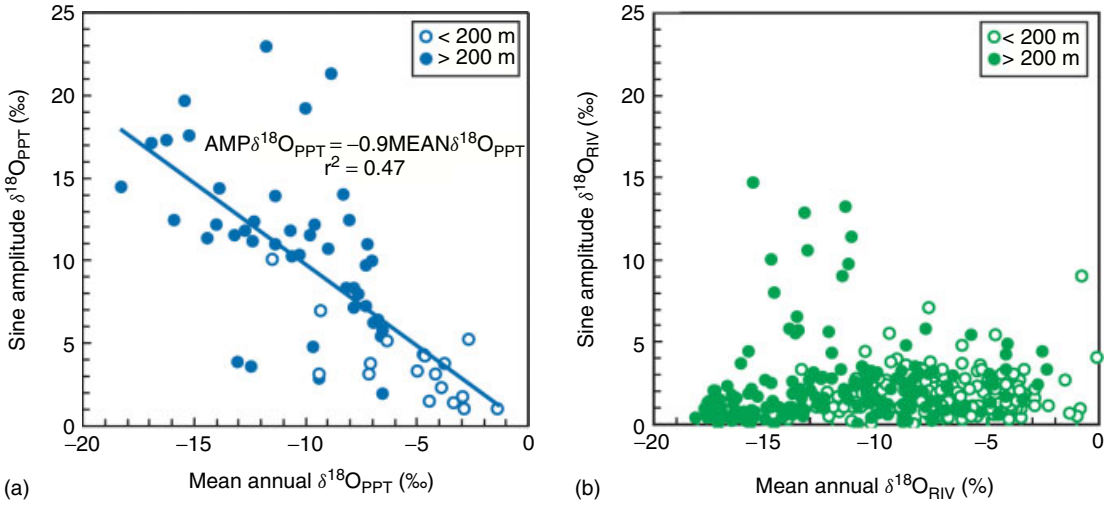

Figure 12. (a) Sinusoid mean annual $\delta^{18}O_{PPT}$ versus sine amplitude of $\delta^{18}O_{PPT}$ at low (open circles) and high (filled circles) elevations. Stations with more negative mean values generally exhibit larger amplitudes of seasonal variation. Seasonal variation increases by about 1‰ for every 1‰ decrease in mean $\delta^{18}O_{PPT}$. (b) Sinusoid mean annual $\delta^{18}O_{RIV}$ versus sine amplitude of $\delta^{18}O_{RIV}$ at low (open circles) and high (filled circles) elevations. Note lack of correlation between mean river water composition and amplitude of seasonal variation. Rivers generally display smaller amplitudes of variation in $\delta^{18}O$ than precipitation. This figure is available in colour online at http://www.interscience.wiley.com/hyp

Bowen and Wilkinson (2002) approach is a significantly better predictor of $\delta^{18}O_{PPT}$ than these alternative methods. The $\delta^{18}O_{PPT}$ map of the USA presented here improves upon that of Bowen and Wilkinson (2002) primarily as a result of increased spatial density of stations, especially across the mid-continent. Even so, future inclusion of more localities will undoubtedly improve our collective understanding of spatial patterns of $\delta^{18}O_{PPT}$ and the processes controlling them.

Because we are most interested here in evaluating differences between maps of $\delta^{18}O_{PPT}$ and $\delta^{18}O_{RIV}$, it is necessary to consider what differences may have been introduced into these maps from our modelling technique. The most significant difference in the generation of these maps is the value used for the apparent lapse rates: −2·9‰ km^{-1} for $\delta^{18}O_{PPT}$ and −4·2‰ for $\delta^{18}O_{RIV}$. To test the sensitivity of this parameter in the model, both lapse rates were set equal at a value of −2·9‰ km^{-1} and maps of $\delta^{18}O_{PPT}$ and $\delta^{18}O_{RIV}$ (similar to Figure 7) were regenerated following the same procedure as before. This simulation still yields more-negative $\delta^{18}O_{RIV}$ values in comparison with $\delta^{18}O_{PPT}$ over the topographically high region of the western USA, very similar to the pattern initially produced in Figure 11. Moreover, the overall spatial patterns of positive and negative anomalies that were initially actualized using different values for lapse rates were reproduced in this simulation. On the basis of this exercise, we conclude that differences in $\delta^{18}O_{PPT}$ and $\delta^{18}O_{RIV}$ lapse rate do not significantly impact the regional extent of similarities and differences between $\delta^{18}O_{PPT}$ and $\delta^{18}O_{RIV}$ across the USA.

Although the lapse rate parameter does not affect the resultant spatial extent of the anomalies, it does impact the magnitude of the anomalies, particularly at higher elevations. Therefore, it is of considerable interest to determine whether the empirically derived $\delta^{18}O_{PPT}$ and $\delta^{18}O_{RIV}$ lapse rates in fact do exhibit a significant difference, or whether, within some acceptable error, the two are really indistinguishable. The different magnitudes of our lapse rates suggest that river water becomes more depleted in ^{18}O with increasing elevation in comparison with the rate of change of $\delta^{18}O_{PPT}$ with elevation. This scenario is entirely plausible if the river water samples are being controlled by a 'catchment effect' and reflect isotopic compositions of $\delta^{18}O_{PPT}$ that fell at higher elevations in the watershed. As intended here, a simple definition of the catchment effect would be that, in an idealized catchment (where $\delta^{18}O_{PPT}$ decreases with increasing elevation and is

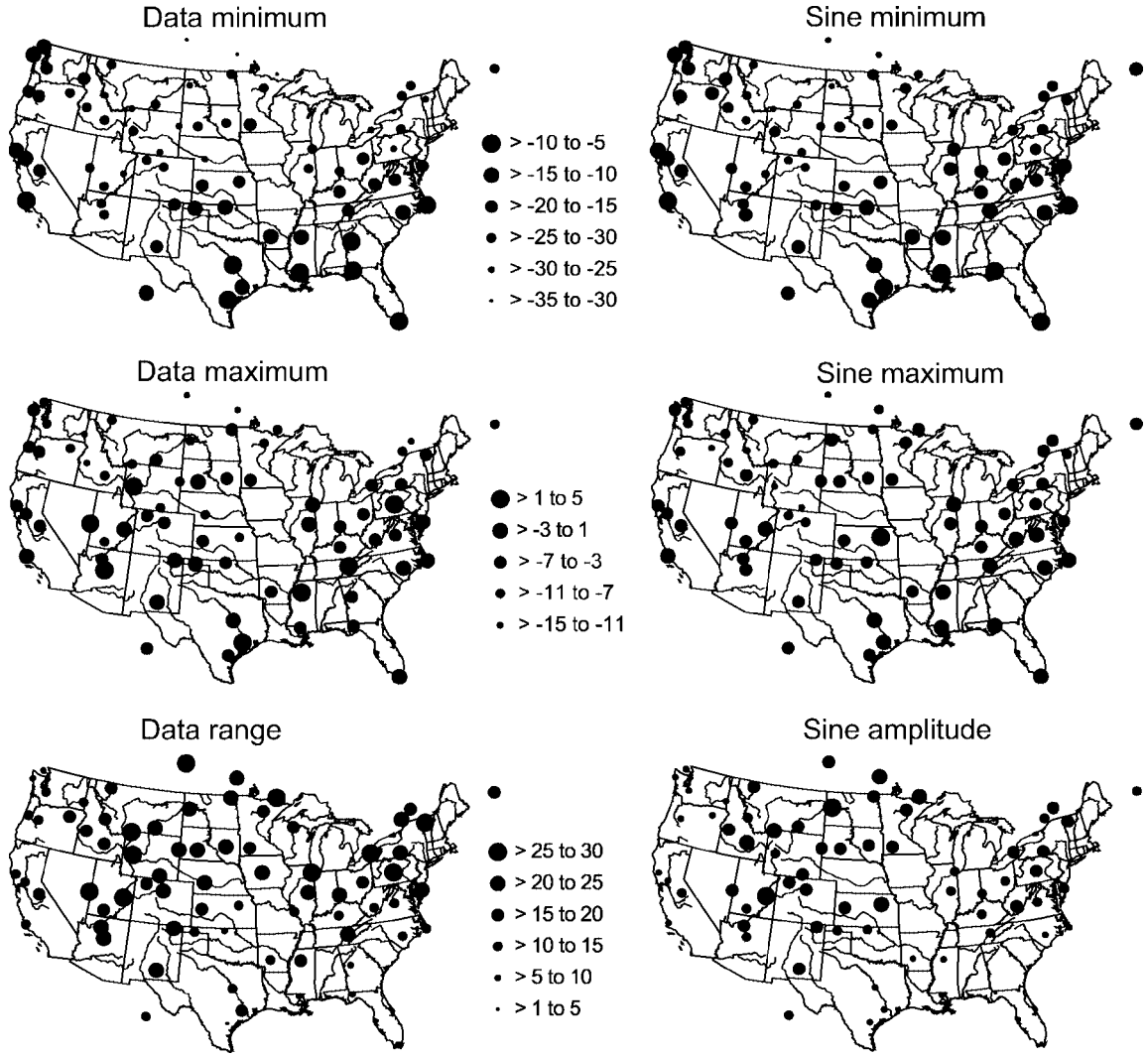

Figure 13. Minimum, maximum, and seasonal variation in $\delta^{18}O_{PPT}$ calculated from station data (left column) and from best-fit sinusoids (right column)

otherwise invariant), $\delta^{18}O_{RIV}$ will be lower than $\delta^{18}O_{PPT}$ at the sampling site by an amount proportional to the difference in elevation between the sampling site and the mean, up-catchment elevation. Because watershed elevation gradients are positively correlated with watershed elevation in the USA, this catchment effect should become more pronounced at higher elevations.

To test this hypothesis, we calculated the expected offset between $\delta^{18}O_{PPT}$ and $\delta^{18}O_{RIV}$ due to the catchment effect by accounting for the elevation and topography of each watershed. If such a catchment effect is indeed the driving mechanism that causes $\delta^{18}O_{RIV}$ to become depleted in ^{18}O at a faster rate than $\delta^{18}O_{PPT}$, then the offset should increase with elevation as watershed gradients become steeper, and the magnitude of the offset should be similar to that predicted by the empirically derived lapse rates.

Watershed elevations and topography were determined for each of the 360 river stations in the Coplen and Kendall (2000) dataset using watersheds mapped in the digital hydrologic unit code (HUC) map of Steeves

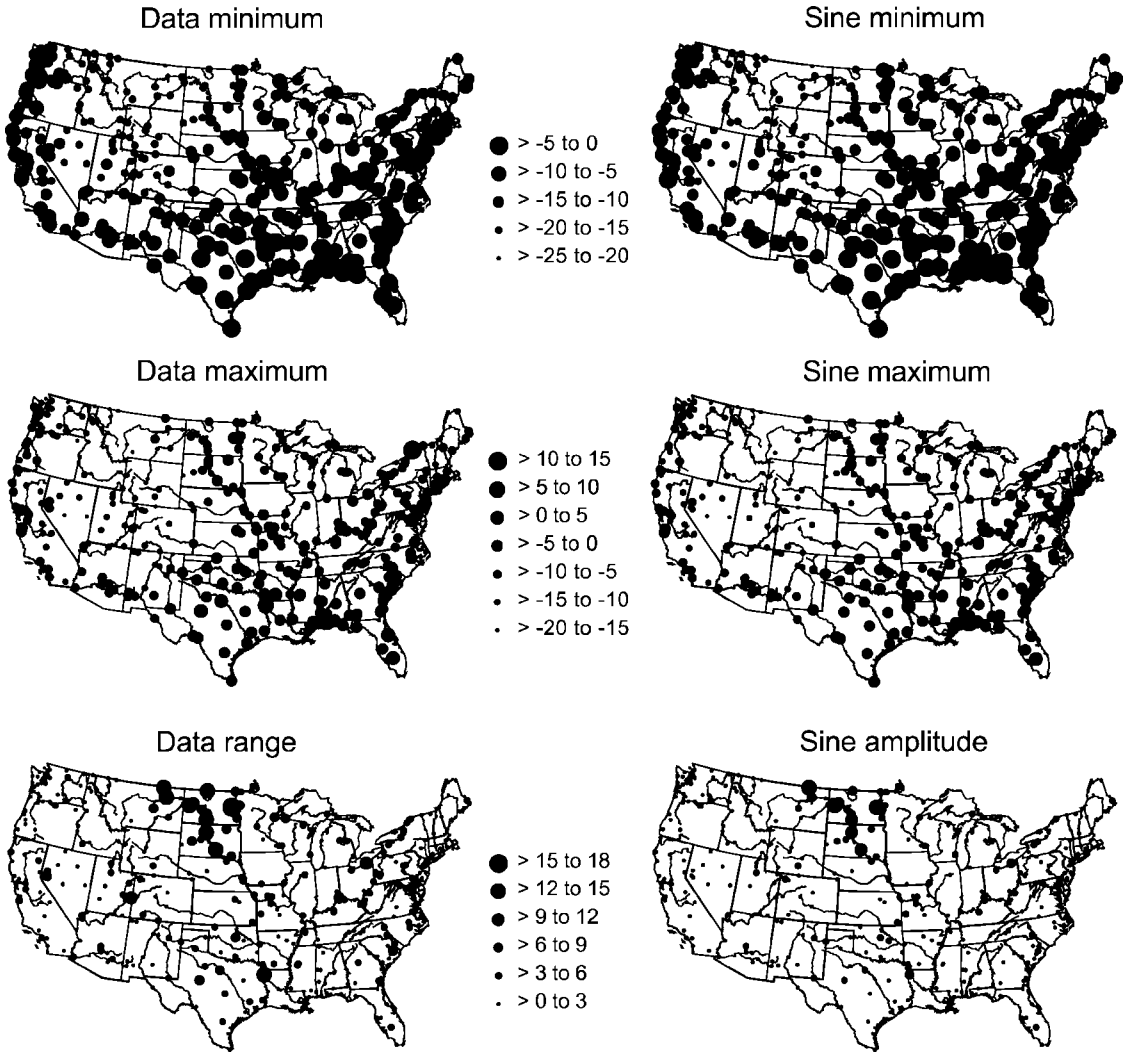

Figure 14. Minimum, maximum, and seasonal variation in $\delta^{18}O_{RIV}$ calculated from station data (left column) and from best-fit sinusoids (right column)

and Nebert (1994) in combination with the GTOPO30 DEM. In this case, we identified a watershed on the basis of the USGS eight-digit HUC label, meaning that we are using a watershed categorization scheme based on relatively small watersheds (average area ~5600 km^2) and not large catchments such as the Mississippi River basin. To calculate the expected offset between $\delta^{18}O_{PPT}$ and $\delta^{18}O_{RIV}$ due to the catchment effect, we assumed that meteoric precipitation is evenly distributed over the watershed and that the river water sample is taken at the outlet of the watershed and represents the average isotopic composition of $\delta^{18}O_{PPT}$ falling in that watershed. Although this somewhat oversimplifies actual drainage basin processes, it is a largely reasonable assumption at the scale of surface flows considered here, and does allow for a first-order estimation of differences between $\delta^{18}O_{PPT}$ and $\delta^{18}O_{RIV}$ values.

Using this model of the catchment effect, $\delta^{18}O_{RIV}$ values were calculated for each of the 360 river stations from the Coplen and Kendall (2000) dataset assuming that river water reflects the average composition of $\delta^{18}O_{PPT}$ over the entire watershed. Comparison of $\delta^{18}O_{RIV}$ and $\delta^{18}O_{PPT}$ over a range of elevations produces

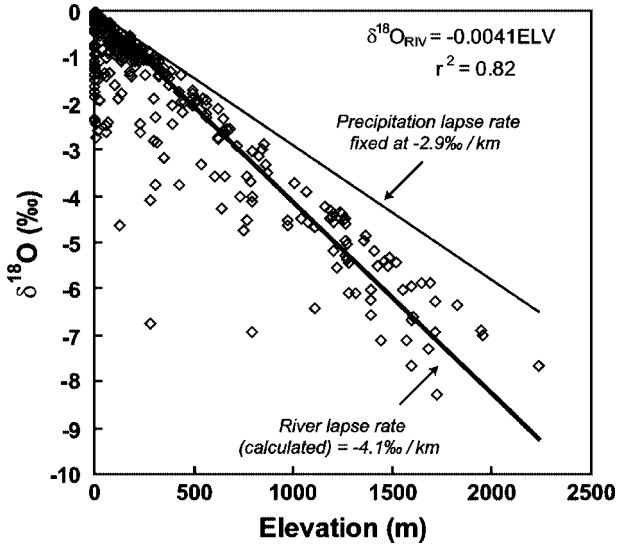

Figure 15. Station elevation versus calculated $\delta^{18}O_{RIV}$ calculated assuming that $\delta^{18}O_{RIV} = \delta^{18}O_{PPT}$ at the average elevation of the eight-digit HUC watershed containing that station. Slope of the linear regression through calculated $\delta^{18}O_{RIV}$ values (thick line) is a 'synthetic' riverine lapse rate of $-4{\cdot}1‰$ km^{-1} for rivers. Precipitation lapse rate (thin line; Figure 4b) is $-2{\cdot}9‰$ km^{-1}. The 'synthetic' riverine lapse rate is almost identical to that measured from river stations ($-4{\cdot}2‰$ km^{-1}), suggesting that differences between $\delta^{18}O_{PPT}$ and $\delta^{18}O_{RIV}$ (Figure 11) primarily reflect more negative precipitation at higher elevations in watersheds

a lapse rate of $-4{\cdot}1‰$ km^{-1} for river water relative to the precipitation lapse rate of $-2{\cdot}9‰$ km^{-1} that was applied to the model (Figure 15). This lapse rate is nearly identical to the empirically derived river water lapse rate of $-4{\cdot}2‰$ km^{-1} that was used in our model of $\delta^{18}O_{RIV}$ values (Equation (6), Figure 8b).

Several interesting deductions can be drawn from this exercise. First, close agreement between the 'synthetic' $\delta^{18}O_{RIV}$ lapse rate derived with the catchment effect model and that calculated from actual river water $\delta^{18}O$ data (Equation (6)) provides verification of the accuracy of this value. Second, because the empirical $\delta^{18}O_{RIV}$ lapse rate was reproduced using a model that invokes a catchment effect control of $\delta^{18}O_{RIV}$, it seems logical to deduce that this process is indeed largely responsible for differences between $\delta^{18}O_{PPT}$ and $\delta^{18}O_{RIV}$ at higher elevations. However, near the top of the watershed, river elevation should increase more quickly than the mean, up-catchment elevation and the two values ($\delta^{18}O_{PPT}$ and $\delta^{18}O_{RIV}$) should approach equality, where the catchment effect is zero. For this reason it is inappropriate to apply a linear model to the river water lapse rate. Yet, owing to the lack of $\delta^{18}O_{RIV}$ data at very high elevations, we are unable to constrain river water compositions in these places and have merely extrapolated the river water, producing an underestimation of $\delta^{18}O_{RIV}$ at high elevations.

Meteoric precipitation

The critical step in generating a map of $\delta^{18}O_{PPT}$ across the USA is to account for regional deviations from the empirically derived latitude–elevation relation (Equation (4)). A few regions within the USA display $\delta^{18}O_{PPT}$ values that are notably different than those calculated from their latitude and elevation. Positive residuals occur over the arid southwest and southern Florida; these represent areas where $\delta^{18}O_{PPT}$ values are more positive than expected (Figure 6). These positive residuals between observed and predicted $\delta^{18}O_{PPT}$ values most likely result from high evaporation rates that cause raindrops to become increasingly enriched in ^{18}O, thus altering the composition of rainwater before collection at the ground surface. In contrast, negative residuals are observed in Idaho, Montana, northern Minnesota, and the northeast. Negative residuals across these northern states likely reflect the importance of Arctic air masses that impart a more negative $\delta^{18}O$ signal

and may also result in part due to the great distance of longitudinal transport of air masses from the West Coast. Interestingly, residuals from the latitude–elevation model are largest at localities characterized by more negative mean annual $\delta^{18}O_{PPT}$ (Figure 5a). These larger residuals occur because these localities are situated at higher latitude or elevation and, therefore, experience a greater range of annual variability in $\delta^{18}O_{PPT}$, which produces a $\delta^{18}O_{PPT}$ signal with more noise than the signal recorded at localities that are lower in elevation or latitude. Although these residuals are substantial in some regions of the country, most of the USA, including the Gulf coast, the Mid-Atlantic States, the Midwest interior, and the West Coast, exhibits residuals with an absolute value less than 1‰.

Both the latitude–elevation dependence of precipitation $\delta^{18}O$ and the regional deviations thereof are accounted for in the final map of $\delta^{18}O_{PPT}$ (Figure 7a). The predominantly east–west orientation of variation in the southeast is contrasted by steep gradients associated with north-south trending contours following the margins of the Cordilleran mountain belt; these lie along the west side of the Sierras (California) and Cascades (Pacific Northwest), and along the east side of the Rocky Mountains.

Although spatial variation in isotope compositions of meteoric precipitation primarily reflects ^{18}O depletion with both latitude and elevation, the map of $\delta^{18}O_{PPT}$ (Figure 7a) is strongly influenced by the location and magnitude of residuals from the latitude-elevation model (Figure 6). For this reason, the $\delta^{18}O_{PPT}$ map is best constrained in areas with a high density of sampling localities.

River water

As with meteoric precipitation, the calculation of regional residuals between observed $\delta^{18}O_{RIV}$ values and values predicted from the latitude–elevation relation for river water $\delta^{18}O$ (Equation (7)) is a crucial step in the generation of the final map of $\delta^{18}O_{RIV}$. These residuals define a broad north–south region of positive residuals that span much of the central Great Plains (Figure 10); here, measured $\delta^{18}O_{RIV}$ values are more positive than would be predicted from latitude and elevation. Moreover, the shape of this positive residual appears to wrap around east of the confluence of the Platte and Missouri rivers in eastern Nebraska, and suggests that these rivers contain water with appreciably different isotopic signatures. Southern Florida, Rhode Island, and Maine also exhibit positive residuals. In contrast, negative residuals occur in the western USA over the Sierra Mountains in California, the Colorado River basin (southwest USA), and the Columbia and Snake river drainages (northwest USA).

Although we used unweighted mean annual $\delta^{18}O_{RIV}$ values, water samples from rivers with substantial base flow are, by their very nature, inherently amount-weighted. For this reason, it is also necessary to consider the seasonal balance of meteoric water fluxes to river systems when evaluating the distribution of river residuals. The north–south-trending band of positive residuals stretching across the Great Plains (Figure 10) is likely due to the dominant influence of the summer Gulf monsoon across this region. The amount of summer precipitation in this area far exceeds the amount of winter precipitation by 20 to 50% (NOAA, 2001) (Figure 16); thus, more positive $\delta^{18}O$ values associated with summer rainfall dominate the $\delta^{18}O_{RIV}$ signal. Central and south Florida are similarly affected by an imbalance between summer and winter precipitation amount (NOAA, 2001), a difference which could explain why river oxygen isotope compositions in this region are more positive than predicted by latitude and elevation. Alternatively, this positive residual could be evidence of evaporative enrichment of river water; this effect has been noted in a study of an east-central Florida watershed by Gremillion and Wanielista (2000). Unfortunately, it is difficult to separate the effects of evaporation and seasonal precipitation in this and other regions of the country.

In contrast to these positive residuals, large regions with negative residuals extend across the western USA (Figure 10). These are likely due to (1) steep elevation gradients in these regions (catchment effect) and (2) the contribution of winter snowmelt to these river systems. In the mountainous western USA, rivers are supplied by ^{18}O-depleted precipitation that condenses at high altitudes. Although an elevation correction is incorporated into $\delta^{18}O_{RIV}$ estimates (Equation (7)), lapse rates may be even larger than $-4{\cdot}2‰\ km^{-1}$ where watershed gradients are steepest. As discussed earlier, additional modelling confirms that differences between

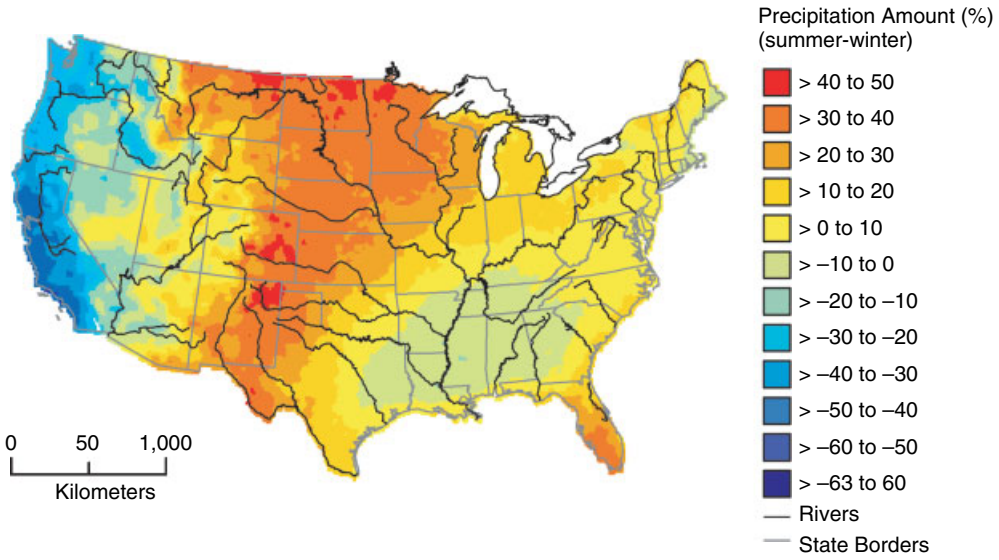

Figure 16. Seasonal balance of precipitation amount calculated from 30-year climate normals (1971–2000) (NOAA, 2001). Annual percentage of summer precipitation minus percentage of winter precipitation is colour coded such that red hues correspond to areas dominated by summer precipitation and blue hues correspond to regions dominated by winter precipitation. Note that the Great Plains receives much more precipitation in the summertime relative to most of the eastern USA, which is relatively balanced between summer and winter precipitation. Data from 7467 stations were interpolated using inverse distance weighting

$\delta^{18}O_{PPT}$ and $\delta^{18}O_{RIV}$ water lapse largely reflect the importance of a catchment effect (see 'Model assessment'). Moreover, many western rivers also experience large seasonal fluxes of ^{18}O-depleted snowmelt, which also contributes to negative $\delta^{18}O_{RIV}$ values. Not surprisingly, the two largest negative $\delta^{18}O_{RIV}$ residuals are centred over two large river basins with headwaters high in the Rocky Mountains, the Columbia–Snake River basin and the Colorado River basin.

These residuals were added to a map of $\delta^{18}O_{RIV}$ values predicted by the latitude–elevation model to provide the final estimate of $\delta^{18}O_{RIV}$ (Figure 7b). Owing to the greater number of river-water sampling stations (360) than precipitation sampling localities (79), spatial variation in $\delta^{18}O_{RIV}$ is generally better constrained than that of $\delta^{18}O_{PPT}$. Kendall and Coplen (2001) generated a contour map across the USA by spatial interpolation of their $\delta^{18}O_{RIV}$ data. In order to compare our map derived from latitude, elevation, and river station data with that of Kendall and Coplen (2001), we colour coded our $\delta^{18}O_{RIV}$ map using the same contour interval (2‰). The two maps are very similar with respect to contour shape and $\delta^{18}O_{RIV}$ magnitude east of the Mississippi River. However, major differences between the two do exist west of the Mississippi. Our map indicates more negative $\delta^{18}O_{RIV}$ values over much of this region and, due to the incorporation of a lapse rate, shows more detail over the topographically elevated (and data-deficient) portions of the western USA.

Superimposed upon patterns produced by change in latitude and elevation is the delivery of river water with relatively negative $\delta^{18}O$ values to areas of lower elevation (Figure 7b). Specifically, areas of more negative $\delta^{18}O_{RIV}$ appear to spread outward from high elevations along vectors of river transport; some down-slope protrusions in negative $\delta^{18}O_{RIV}$ appear to track major river systems, and are particularly evident along the Missouri River near the South Dakota–Nebraska border, the Yellowstone River across western Montana, and the Rio Grande along the southern border of western Texas.

Another rather striking aspect of this $\delta^{18}O_{RIV}$ map is that river compositions lighter than −20‰ occupy a significantly greater area across the western interior of the USA than do equally depleted compositions of meteoric precipitation (Figure 7). It is important to note here that over much of this region the compositions of river water are largely unconstrained by field measurements, and very negative $\delta^{18}O_{RIV}$ values are interpolated

to occur in high-elevation regions that lie between data stations where somewhat less negative measurements (−16 to −20‰) are reported. In theory, at the summits of mountains (at the highest elevations in the highest watersheds), $\delta^{18}O$ of precipitation and rivers (if they exist) should be equal. We therefore expect that, at the highest elevations, the linear lapse rate for $\delta^{18}O_{RIV}$ underestimates isotopic values, and $\delta^{18}O_{RIV}$ values should approach those of local $\delta^{18}O_{PPT}$.

In considering the compositions of river water, we have neglected to quantify the potential isotopic effects of dams, which are present in many of the rivers included in this study. Reservoirs associated with these dams may generate evaporative effects (enrichment of ^{18}O) and may also produce smaller magnitudes in seasonality downstream from the dam. Another consideration for the river water data is that seasonally ephemeral rivers and/or higher order rivers (smaller rivers than those included in this study) may be associated with different isotopic characteristics than the rivers considered here.

Comparison of precipitation and riverine $\delta^{18}O$

Significant differences between river and precipitation compositions ($\delta^{18}O_{RIV} - \delta^{18}O_{PPT}$) are observed across the USA (Figure 11). These differences record spatial variation in the balance of precipitation and evaporation, the seasonal balance of precipitation amount, and topography of the watershed, which in turn determines magnitude of catchment effects on river water samples. Positive anomalies ($\delta^{18}O_{RIV} > \delta^{18}O_{PPT}$) are generally 1 to 3‰ in magnitude, but range up to ~5‰. A larger area of the USA is characterized by negative anomalies ($\delta^{18}O_{RIV} < \delta^{18}O_{PPT}$) that generally have values of −1 to −7‰. In contrast, little to no difference between $\delta^{18}O_{RIV}$ and $\delta^{18}O_{PPT}$ is observed across most of the eastern USA.

A discontinuous band of positive anomalies trends north–south across the Great Plains from Texas to northernmost Minnesota and the Dakotas. This anomaly is interpreted as resulting from seasonal imbalance in amounts of meteoric precipitation, because the region is characterized by a much higher percentage of summer than winter precipitation (NOAA, 2001). Owing to the fact that rivers are fed both by groundwater and precipitation-related surface flow, short-term values of $\delta^{18}O_{RIV}$ are potentially affected by a flux of average groundwater $\delta^{18}O$ (a homogenized signal of precipitation) and by the $\delta^{18}O$ values of seasonal precipitation. As a result, $\delta^{18}O_{RIV}$ is inherently weighted by precipitation amount. Positive anomalies across the Great Plains could also reflect some additional influence of evaporation (which would preferentially remove ^{16}O from surface river waters).

Although we might expect the effect of evaporation on $\delta^{18}O_{RIV}$ to be most pronounced in arid areas such as the Southwest, $\delta^{18}O_{RIV}$ is predominantly more negative than $\delta^{18}O_{PPT}$ in this region. This region is within part of a large negative anomaly that covers the entire western half of the USA (Figure 11) and is attributed to the combined effects of isotopically negative snowmelt feeding major river systems, and steep topographic gradients that deliver ^{18}O-depleted precipitation to river sampling localities at lower elevations. This result is not particularly surprising given prior observations that large rivers in arid catchment basins, such as the Colorado River in the southwest USA, can retain isotopic compositions depleted in ^{18}O that originated outside the catchment basin (Friedman *et al*., 1992; Ingraham *et al*., 1998). Additionally, several other studies of local catchments have demonstrated that river and/or groundwater $\delta^{18}O$ can be significantly depleted in ^{18}O relative to local precipitation owing to greater contribution from winter precipitation $\delta^{18}O$ (Fritz *et al*., 1987; Ingraham and Taylor, 1991; Maulé *et al*., 1994; Simpkins, 1995; Winograd *et al*., 1998). This contribution may be achieved in areas where annual precipitation amount is biased towards winter precipitation, such as along the entire western coast of the USA (NOAA, 2001). Alternatively, even if seasonal precipitation amount is relatively balanced, winter precipitation might preferentially infiltrate the soil under the winter snowpack, and consequently have a greater influence on both groundwater and river water oxygen isotope composition (Ingraham and Taylor, 1991; Simpkins, 1995). Furthermore, rivers with headwaters at high elevations that are perennially fed by glaciers and/or snowmelt would display an average isotopic composition biased towards those compositions.

Another factor that may also contribute to the large negative anomaly over the western USA is that the catchment effect is in fact larger than that incorporated into our model. Topographic relief in the USA is

highest across the Rocky Mountains, and the catchment effect should be stronger across this region as well. If so, this would result in a larger difference between $\delta^{18}O_{RIV}$ and local $\delta^{18}O_{PPT}$.$\delta^{18}O_{RIV}$ would, therefore, be more negative, because it would reflect precipitation compositions from higher elevations in the watershed. Undoubtedly, some combination of these mechanisms is responsible for the large negative anomaly over the western USA.

One particularly notable aspect of the negative anomaly in the western USA is a bulge that extends to the east, following the Missouri and Platte rivers across North Dakota, South Dakota, and Nebraska (Figure 11). These two major rivers have their headwaters at high elevations farther to the north and west, near the Continental Divide, where the dominant source vapour is from the Pacific (Bryson and Hare, 1974). As a result, they transport water to the east that is more ^{18}O-depleted than Great Plains precipitation, which is largely sourced from the Gulf of Mexico. In addition, these rivers are dominantly supplied by snowmelt at higher elevations that may further contribute to the relatively negative $\delta^{18}O$ values of these rivers.

Most of the eastern USA shows no difference ($\pm 1‰$) between $\delta^{18}O_{PPT}$ and $\delta^{18}O_{RIV}$. Exceptions to this generalization include slight $\delta^{18}O_{RIV}$ enrichment in southern Florida and along coastal New England (Figure 11). These positive anomalies are relatively small, and may reflect the influence of precipitation sourced from warm Gulf Stream waters.

Seasonality in meteoric $\delta^{18}O$

In addition to the comparison of mean annual isotopic compositions, there is also considerable interest in understanding modern relations between seasonal ranges of $\delta^{18}O_{RIV}$ and $\delta^{18}O_{PPT}$. Seasonal amplitudes of $\delta^{18}O_{RIV}$ (both sine amplitude and absolute range) are generally quite small; 94% of river stations have sinusoid amplitudes $<5‰$. River stations with the largest seasonal change in $\delta^{18}O$ composition are located in the upper Midwest, along the upper reaches of the Missouri River in North Dakota, South Dakota, and northeastern Montana (Figure 14). This large seasonal signal appears to be driven by extremely negative winter values of $\delta^{18}O_{RIV}$.

Seasonality in $\delta^{18}O_{PPT}$ generally exhibits a much wider range of values than $\delta^{18}O_{RIV}$, and appears to be smaller along coastal regions than in the continental interior (Figure 13). Seasonal variation in temperature (and hence in $\delta^{18}O_{PPT}$) is generally understood to increase with increasing latitude, where there is greater variation in the amount of solar insolation. This relation between mean annual temperature and amplitude of seasonal temperature variation is reflected in some negative correlation between sinusoid amplitude of $\delta^{18}O_{PPT}$ and mean annual $\delta^{18}O_{PPT}$ (Figure 12). Suppression of seasonality in $\delta^{18}O_{RIV}$ change relative to that of precipitation is undoubtedly due to the longer residence time of groundwater relative to precipitation-related overland flow, and the attendant averaging effect that this has on compositions of groundwaters that feed most river systems. It is also important to note here that ephemeral streams and rivers may display greater and more uncorrelated variation in the $\delta^{18}O$ signal than is apparent in the rivers included in this study.

Application of results to palaeoclimate studies

Ultimately, maps of spatial variation in $\delta^{18}O_{PPT}$ and $\delta^{18}O_{RIV}$ provide insight into those processes that serve to modify compositions of meteoric precipitation that in turn feed regional river drainage systems. As such, they have potentially broad application to the interpretation of isotope compositions of biogenic hard parts accreted in riverine and/or lacustrine settings that serve as archives of meteoric $\delta^{18}O$ and ancient climate. Such maps provide continuous spatial estimates of both modern $\delta^{18}O_{RIV}$ and $\delta^{18}O_{PPT}$, even in regions lacking modern $\delta^{18}O$ measurements. Moreover, several regionally important processes not directly related to either latitude or elevation serve to modify $\delta^{18}O_{PPT}$ as water moves from precipitation–surface flow to ground–river water reservoirs. To the degree that these processes were also important in analogous ancient environments, maps of modern precipitation should lead to a better interpretation of fossil proxy data.

This study highlights two important considerations for palaeoenvironmental studies. First, significant differences can exist between annual average $\delta^{18}O_{PPT}$ and $\delta^{18}O_{RIV}$, even when seasonal precipitation amount

is considered. Second, the significant difference that exists between seasonal variation $\delta^{18}O_{PPT}$ and $\delta^{18}O_{RIV}$ implies that biogenic hard parts accreted in isotopic equilibrium with river water will, at best, record only a small fraction of seasonal variation in $\delta^{18}O_{PPT}$ and, by implication, seasonal variation in temperature.

Bearing these results in mind, we must also consider that spatial variation in $\delta^{18}O_{PPT}$ and $\delta^{18}O_{RIV}$ across the USA undoubtedly would have been somewhat different in the geologic past. Over long periods of time, uplift and denudation of orogenic belts will influence the effect of adiabatic uplift of continental air masses and, therefore, the amount of concomitant depletion of ^{18}O in meteoric precipitation. Change in $\delta^{18}O$ over long time scales has been used to estimate both the amount (Drummond *et al*., 1993) and timing (Rowley *et al*., 2001; Kohn *et al*., 2002) of mountain uplift. Moreover, latitudinal gradients in meteoric $\delta^{18}O$ may respond to changes in climate dynamics on seasonal time scales or between ancient and modern climate states (Fricke and O'Neil, 1999; Ufnar *et al*., 2002).

Given the potential for regional change in $\delta^{18}O_{PPT}$ and $\delta^{18}O_{RIV}$ values over time, it is of course critical, first, to understand modern distributions of $\delta^{18}O_{PPT}$, and to understand further the relations between $\delta^{18}O_{PPT}$ and other meteoric water reservoirs and/or compositions of modern proxies, before attempting interpretation of ancient palaeoclimate data. Although this system is complicated, careful analysis of proxy data, combined with consideration of the processes highlighted in this study (e.g. catchment effect) that can influence other reservoirs of meteoric water, has the potential to provide important and meaningful constraints on palaeoclimate and palaeoelevation.

To illustrate this point, we consider the results of Ufnar *et al*. (2002) in light of the results of our study. Ufnar *et al*. (2002) have taken a promising step toward the construction of a mid-Cretaceous (Albian) $\delta^{18}O_{PPT}$–latitude gradient based on $\delta^{18}O$ compositions of pedogenic siderite nodules. Ufnar *et al*. (2002) report more depleted $\delta^{18}O_{PPT}$ values for the Albian relative to modern compositions at similar latitudes, as well as a steeper $\delta^{18}O_{PPT}$–latitude gradient in comparison with modern precipitation. Although this line of research provides greater insight into the controls of climate upon the meteoric $\delta^{18}O$ signal for ancient climates, it is also essential to determine whether siderite nodule compositions (modern or ancient) record north–south gradients in the compositions of meteoric precipitation, or whether they more closely record latitudinal changes in the compositions of local ground and/or river waters. This is an important distinction, because we find that the modern $\delta^{18}O_{RIV}$–latitude gradient (Equation (7)) is steeper than that of modern $\delta^{18}O_{PPT}$, and the difference between these slopes is similar to the difference in slopes between the Albian latitudinal gradient (based on siderite nodule data) and the modern theoretical siderite nodule gradient (Ufnar *et al*., 2002). This raises an important point for both modern and ancient studies of meteoric $\delta^{18}O$: the combination of measurements (or proxies) of precipitation $\delta^{18}O$ should be considered separately from other reservoirs of meteoric water (e.g. rivers, lakes, and groundwater), as these reservoirs are subject to different processes that may alter their oxygen isotope composition. The potential importance of these processes is evidenced by the significant differences between modern river water and precipitation that are highlighted in this study.

CONCLUSIONS

Determination of relations between meteoric water $\delta^{18}O$, latitude, elevation, and a number of regional effects allow for the generation of 30 arc-second maps of (1) $\delta^{18}O$ of precipitation (Figure 7a), (2) $\delta^{18}O$ of river water (Figure 7b), and (3) difference between water compositions in these two reservoirs (Figure 11). Broad regions across the USA, particularly the Great Plains and the western USA, exhibit significant differences between mean annual $\delta^{18}O_{PPT}$ and $\delta^{18}O_{RIV}$ that are driven primarily by differences in the elevation of catchment areas and river-water sampling stations, as well as by seasonal biasing due to differences in amount of precipitation and/or amount of snowpack infiltration. Although oxygen isotope compositions of river water and groundwater are similar across broad regions of the eastern USA, river water is enriched in ^{18}O relative to precipitation across much of the Great Plains, as well as smaller areas along the eastern seaboard, and

is significantly depleted in ^{18}O across much of the western USA. Maps of seasonal variation in $\delta^{18}O$ for both precipitation and river water displayed as point data at each measurement locality (Figures 13 and 14) indicate that differences between local $\delta^{18}O_{PPT}$ and $\delta^{18}O_{RIV}$ seasonality can be quite large. Seasonal variation in the annual $\delta^{18}O$ signal is significantly larger than that of local river water.

These differences suggest that caution should be made when lumping $\delta^{18}O$ analyses from different types of palaeoclimatological proxies. Significant differences exist between $\delta^{18}O$ values of local precipitation when compared with those of through flowing rivers. Regional variation in the magnitude and sign of these differences can helpful in interpreting proxy data for meteoric $\delta^{18}O$ in both modern and ancient systems. Other reservoirs of meteoric water, such as groundwater, soil porewater, and lake water that are not directly represented by the analyses of meteoric precipitation and river water considered here, may also display patterns of regional variation in oxygen isotope compositions that result from processes more-or-less unique to these systems. However, significantly more modern data are needed to evaluate these patterns on a large scale.

Finally, this study provides evidence that palaeoenvironmental studies should not assume that river water $\delta^{18}O$ is identical to that of precipitation $\delta^{18}O$ when making palaeoclimatic interpretations. Although large regions of the USA are characterized by $\delta^{18}O_{PPT}$ and $\delta^{18}O_{RIV}$ values that are effectively equal, almost equally large regions display significant differences between these two parameters. We suggest that, despite these complications, proxy data for meteoric water can still be a valuable and reliable means for reconstructing palaeoelevation or palaeoclimate by considering the processes discussed in this study that generate differences between separate reservoirs of meteoric water. As such, our comparison between modern river water and meteoric precipitation has the potential to improve our collective ability to evaluate palaeoclimates, and to enhance our understanding of ancient climate systems.

ACKNOWLEDGEMENTS

We would like to thank two anonymous reviewers for their improvements to the manuscript, and D. Seigel and K. Lambeck for helpful reviews of earlier versions of this manuscript. This work has also benefited from discussions with B. McElroy, C. Badgely, S. Wing, G. Smith, and D. Fox. A National Science Foundation Graduate Research Fellowship and a Rackham Pre-doctoral Fellowship to A.D. supported this research. We also wish to acknowledge the NSF-Earth System History Program (ATM-0196475) for supporting the USNIP program and J.W.'s contribution. Some of the precipitation samples used in this analysis were provided by the National Atmospheric Deposition Program (a cooperative research support program of federal, state, local, and tribal agencies), State Agricultural Experiment Stations, universities, national laboratories, and non-governmental organizations (see http://nadp.sws.uiuc.edu).

REFERENCES

Amundson R, Chadwick O, Kendall C, Wang Y, DeNiro M. 1996. Isotopic evidence for shifts in atmospheric circulation patterns during the late Quaternary in mid-North America. *Geology* **24**(1): 23–26.

Bao H, Koch P. 1999. Oxygen isotope fractionation in ferric oxide–water systems; low temperature synthesis. *Geochimica et Cosmochimica Acta* **63**(5): 599–613.

Bao H, Koch P, Hepple RP. 1998. Hematite and calcite coatings on fossil vertebrates. *Journal of Sedimentary Research* **68**(5): 727–738.

Bowen GJ, Revenaugh J. 2003. Interpolating the isotopic composition of modern meteoric precipitation. *Water Resources Research* **39**(10): DOI: 10·1029/2003WR002086.

Bowen GJ, Wilkinson BH. 2002. Spatial distribution of $\delta^{18}O$ in meteoric precipitation. *Geology* **30**(4): 315–318.

Bryant JD, Koch PL, Froelich PN, Showers WJ, Genna BJ. 1996. Oxygen isotope partitioning between phosphate and carbonate in mammalian apatite. *Geochimica et Cosmochimica Acta* **60**: 5145–5148.

Bryson RA, Hare FK. 1974. The climate of North America. In *Climates of North America*, Bryson RA, Hare FK (eds). Elsevier: New York; 1–47.

Cerling TE, Quade J. 1993. Stable carbon and oxygen isotopes in soil carbonates. In *Climate Change in Continental Isotopic Records*, Swart PK, Lohmann KC, McKenzie JA, Savin S (eds). American Geophysical Union: Washington, DC; 217–231.

Chamberlain CP, Poage MA. 2000. Reconstructing the paleotopography of mountain belts from the isotopic composition of authigenic minerals. *Geology* **28**(2): 115–118.

Coplen TB. 1993. Uses of environmental isotopes. In *Regional Ground-Water Quality*, Alley WB (ed). Van Nostrand Reinhold: New York; 227–254.
Coplen TB, Huang R. 2000. Stable hydrogen and oxygen isotope ratios for selected sites of the National Oceanic and Atmospheric Administration's Atmospheric Integrated Research Monitoring Network (AiRMoN). US Geological Survey Open File Report 00-279: Reston; 54pp.
Coplen TB, Kendall C. 2000. Stable hydrogen and oxygen isotope ratios for selected sites of the US Geological Survey's NASQAN and Benchmark surface-water networks. US Geological Survey Open File Report 00-160: Reston; 409pp.
Dansgaard W. 1964. Stable isotopes in precipitation. *Tellus* **XVI**: 436–468.
Dansgaard W, Johansen SJ, Clausen HB, Dahl-Jensen D, Gundestrup NS, Hammer CU, Hvidberg CS, Steffensen JP, Sveinbjornsdottir AE, Jouzel J, Bond G. 1993. Evidence for general instability of past climate from a 250-kyr ice-core record. *Nature* **364**: 218–220.
Denniston RF, Gonzalez LA, Asmerom Y, Baker RG, Reagan MK, Bettis EA III. 1999. Evidence for increased cool season moisture during the middle Holocene. *Geology* **27**: 815–818.
Dettman DL, Lohmann KC. 2000. Oxygen isotope evidence for high-altitude snow in the Laramide Rocky Mountains of North America during the Late Cretaceous and Paleogene. *Geology* **28**(3): 243–246.
Dorale JA, Gonzalez LA, Reagan MK, Pickett DA, Murrell MT, Baker RG. 1992. A high-resolution record of Holocene climate change in speleothem calcite from Cold Water Cave, northeast Iowa. *Science* **258**: 1626–1630.
Drummond CN, Wilkinson BH, Lohmann KC, Smith GR. 1993. Effect of regional topography and hydrology on the lacustrine isotopic record of Miocene paleoclimate in the Rocky Mountains. *Palaeogeography, Palaeoclimatology, Palaeoecology* **101**(1–2): 67–79.
Dutton AR. 1995. Groundwater isotopic evidence for paleorecharge in the High Plains aquifers. *Quaternary Research* **43**: 221–231.
Frederickson GC, Criss RE. 1999. Isotope hydrology and residence times of the unimpounded Meramec River basin, Missouri. *Chemical Geology* **157**: 303–317.
Fricke HC, O'Neil Jr. 1999. The correlation between $^{18}O/^{16}O$ ratios of meteoric water and surface temperature: its use in investigating terrestrial climate change over geologic time. *Earth and Planetary Science Letters* **170**: 181–196.
Fricke HC, Clyde WC, O'Neil Jr. 1998. Intra-tooth variations in $\delta^{18}O(PO_4)$ of mammalian tooth enamel as a record of seasonal variations in continental climate variables. *Geochimica et Cosmochimica Acta* **62**: 1839–1850.
Friedman I, Smith GI, Gleason JD, Warden A, Harris JM. 1992. Stable isotope composition of waters in southeastern California, 1. Modern precipitation. *Journal of Geophysical Research* **97**(D5): 5795–5812.
Fritz P, Drimmie RJ, Frape SK, O'Shen K. 1987. The isotopic composition of precipitation and groundwater in Canada. In *Isotope Techniques in Water Resources Development*, IAEA (ed.). IAEA: Vienna; 539–550.
Gat J, Matsui E. 1991. Atmospheric water balance in the Amazon basin: an isotopic evapotranspiration model. *Journal of Geophysical Research* **96**(D7): 13 179–13 188.
Gonfiatini R. 1978. Standards for stable isotope measurements in natural compounds. *Nature* **271**: 534–536.
Gremillion P, Wanielista M. 2000. Effects of evaporative enrichment on the stable isotope hydrology of a central Florida (USA) river. *Hydrological Processes* **14**: 1465–1484.
Harvey FE, Welker JM. 2000. Stable isotopic composition of precipitation in the semi-arid north-central portion of the US Great Plains. *Journal of Hydrology* **238**: 90–109.
Hays PD, Grossman EL. 1991. Oxygen isotopes in meteoric calcite cements as indicators of continental paleoclimate. *Geology* **19**: 441–444.
IAEA/WMO. 2001. Global Network of Isotopes in Precipitation. The GNIP Database. http://isohis.iaea.org [24 Jun 2005].
Ingraham NL, Taylor BE. 1991. Light stable isotope systematics of large-scale hydrologic regimes in California and Nevada. *Water Resources Research* **27**(1): 77–90.
Ingraham NL, Caldwell EA, Verhagen B. 1998. Arid catchments. In *Isotope Tracers in Catchment Hydrology*, Kendall C, McDonnell JJ (eds). Elsevier: Amsterdam; 435–465.
Kendall C. 1993. *Impact of isotopic heterogeneity in shallow systems on stormflow generation*. PhD dissertation, University of Maryland, College Park.
Kendall C, Coplen TB. 2001. Distribution of oxygen-18 and deuterium in river waters across the United States. *Hydrological Processes* **15**: 1363–1393.
Kohn MJ, Miselis JL, Fremd TJ. 2002. Oxygen isotope evidence for progressive uplift of the Cascade Range, Oregon. *Earth and Planetary Science Letters* **204**(1–2): 151–165.
Krabbenhoft DP. 1990. Estimating groundwater exchange with lakes, 1. The stable isotope mass balance method. *Water Resources Research* **26**(10): 2445–2453.
Lawrence JR, White JC. 1991a. The elusive climate signal in the isotopic composition of precipitation. In *Stable Isotope Geochemistry; a Tribute to Samuel Epstein*, Taylor HP, O'Neil JR, Kaplan IR (eds). Geochemical Society: University Park, PA; 169–185.
Maulé CP, Chanasyk DS, Muehlenbachs K. 1994. Isotopic determination of snow-water contribution to soil water and groundwater. *Journal of Hydrology* **155**: 73–91.
Nativ R, Riggio R. 1990. Precipitation in the southern High Plains: meteorologic and isotopic features. *Journal of Geophysical Research* **95**(D13): 22 559–22 564.
NOAA. 2001. Climatography of the United States No.81, Climate Normals 1971–2000. National Oceanic and Atmospheric Administration: Asheville, NC, USA.
Petit JR, Jouzel J, Raynaud D, Barkov MI, Barnola JM, Basile I, Bender M, Chappellaz J, Davis M, Delaygue G, Delmotte M, Kotlyakov VM, Legrand M, Lipenkov VY, Lorius C, Pepin L, Ritz C, Saltzmann E, Stievenard M. 1999. Climate and atmospheric history of the past 420,000 years from the Vostok ice core, Antarctica. *Nature* **399**: 429–436.
Poage MA, Chamberlain CP. 2001. Empirical relationships between elevation and the stable isotope composition of precipitation and surface waters: considerations for studies of paleoelevation change. *American Journal of Science* **301**: 1–15.
Rowley D, Pierrehumbert RT, Currie BS. 2001. A new approach to stable isotope-based paleoaltimetry: implications for paleoaltimetry and paleohypsometry of the High Himalaya since the Late Miocene. *Earth and Planetary Science Letters* **188**: 253–268.

Rozanski K. 1985. Deuterium and oxygen-18 in European groundwaters; links to atmospheric circulation in the past. *Chemical Geology* **52**: 349–363.
Rozanski K, Araguas-Araguas L, Gonfiantini R. 1993. Isotopic patterns in modern global precipitation. In *Climate Change in Continental Isotopic Records*, Swart P, Lohmann KC, McKenzie JA, Savin S (eds). American Geophysical Union: Washington, DC; 1–36.
Salati E, Dall'Olio A, Matsui E, Gat Jr. 1979. Recycling of water in the Amazon basin: an isotopic study. *Water Resources Research* **15**(5): 1250–1258.
Schwarz HP. 1986. Geochronology and isotopic geochemistry of speleothems. In *Handbook of Environmental Isotope Geochemistry*, Fritz P, Fontes JC (eds). Elsevier: Amsterdam; 271–304.
Sharp ZD, Cerling TE. 1998. Fossil isotope records of seasonal climate and ecology—straight from the horse's mouth. *Geology* **26**: 219–222.
Sheppard SMF, Nielsen RL, Taylor HP. 1969. Oxygen and hydrogen isotope ratios of clay minerals from porphyry copper deposits. *Economic Geology* **64**: 755–777.
Simpkins WW. 1995. Isotopic composition of precipitation in central Iowa. *Journal of Hydrology* **172**: 185–207.
Simpson HJ, Herczeg AL. 1991. Stable isotopes as an indicator of evaporation in the River Murray, Australia. *Water Resources Research* **27**: 1925–1935.
Steeves P, Nebert D. 1994. Hydrologic maps of the conterminous United States. US Geological Survey Open-File Report: Reston; 94-0236.
Thompson LG, Mosley-Thompson E, Daviss ME, Lin PN, Henderson KA, Cole-Dai J, Bolzan JF, Liu KB. 1995. Late glacial stage and Holocene tropical ice core records from Huscaran, Peru. *Science* **269**: 46–50.
Ufnar DF, Gonzalez LA, Ludvigson GA, Brenner RL, Witzke BJ. 2002. The mid-Cretaceous water bearer: isotope mass balance quantification of the Albian hydrologic cycle. *Palaeogeography, Palaeoclimatology, Palaeoecology* **188**: 51–71.
Welker JM. 2000. Isotopic (δ^{18}O) characteristics of weekly precipitation collected across the USA: an initial analysis with application to water source studies. *Hydrological Processes* **14**: 1449–1464.
Welker JM, White JC, Vachon R, Esposito D, Larson R. 2002. High resolution spatial patterns of the isotopic characteristics of precipitation across the U.S. during El Nino and La Nina phases. *EOS Transactions* **83**: (47).
Wilkinson BH, Ivany L. 2002. Paleoclimatic inference from stable isotope profiles of accretionary biogenic hardparts—a quantitative approach to the evaluation of incomplete data. *Palaeogeography, Palaeoclimatology, Palaeoecology* **185**: 95–114.
Winograd IJ, Riggs AC, Coplen TB. 1998. The relative contributions of summer and cool-season precipitation to groundwater recharge, Spring Mountains, Nevada, USA. *Hydrogeology Journal* **6**: 77–93.
Wurster CM, Patterson WP. 2001. Late Holocene climate change for the eastern interior United States; evidence from high-resolution δ^{18}O values of sagittal otoliths. *Palaeogeography, Palaeoclimatology, Palaeoecology* **170**(1–2): 81–100.
Yurtsever Y, Gat Jr. 1981. Atmospheric waters. In *Stable Isotope Hydrology: Deuterium and Oxygen-18 in the Water Cycle*, Gat JR, Gonfiantini R (eds). International Atomic Energy Association: Vienna; 103–139.

